Summer 1-1-2020

Surface Functionalization And Optical Spectroscopy of Singlewall Carbon Nanotubes

Fjorela Xhyliu
Cleveland State University

SURFACE FUNCTIONALIZATION AND OPTICAL SPECTROSCOPY OF SINGLE-WALL CARBON NANOTUBES

FJORELA XHYLIU

Bachelor of Chemical Engineering

Cleveland State University

August 2019

Submitted in partial fulfillment of requirements for the degree

MASTER OF SCIENCE IN BIOMEDICAL ENGINEERING

at

CLEVELAND STATE UNIVERSITY

August 2020

We hereby approve the thesis for

FJORELA XHYLIU

Candidate for the Master of Science in Biomedical Engineering degree for the

Department of Chemical and Biomedical Engineering

And CLEVELAND STATE UNIVERSITY'S

College of Graduate studies by

Thesis Chairperson, Dr. Geyou Ao
Department of Chemical and Biomedical Engineering

_____
Date

Thesis Committee Member, Dr. Xue-Long Sun
Department of Chemistry

_____
Date

Thesis Committee Member, Dr. Moo-Yeal Lee
Department of Chemical and Biomedical Engineering

_____
Date

Date of Defense: July 21, 2020

ACKNOWLEDGMENTS

First and foremost, I would like to thank Dr. Geyou Ao for giving me the opportunity to work in her lab. Joining your lab was one of the most rewarding decisions I have ever made. Thank you for your continuous support and guidance, for turning a college sophomore with no life direction into the professional that I am today.

I would like to thank Dr. Xue-Long Sun and Dr. Moo-Yeal Lee for their useful feedback on my thesis and during this collaboration. I would also like to express my appreciation to everyone in the department for all their miscellaneous help.

I would like to acknowledge my friends for being with me throughout my college journey and helping with life in general. Also, thank you to my lab mates for making my time in the lab more enjoyable at times and for your constructive feedback.

Thank you, Thomas, for your unconditional support and motivation.

Most importantly, I want to thank my mother and my family for their tremendous support in advancing my education. Thank you to my parents for raising me most humbly and teaching me not to live life too ambitiously. I am especially thankful to my father whose memory is always with me. I will be forever grateful for being born as your daughter.

SURFACE FUNCTIONALIZATION AND OPTICAL SPECTROSCOPY OF SINGLE-WALL CARBON NANOTUBES

FJORELA XHYLIU

ABSTRACT

This thesis describes a comprehensive study on the complexation of single-wall carbon nanotubes (SWCNTs) with biopolymers via noncovalent and covalent approaches as well as the characterization of the resulting complexes. SWCNTs are unique, one-dimensional nanocylinders that are highly attractive for surface modification because all their atoms comprise a surface. Specifically, single-chirality SWCNTs functionalized with biomolecules are excellent candidates for applications in bioimaging, biochemical sensing, and drug delivery. Here, we investigated the complexation affinity of recognition sequences of single-stranded DNA (ssDNA) with SWCNTs. We utilized the optical modulation of ten chirality-pure SWCNTs to study the kinetics of the coating displacement of ssDNA by a strong surfactant. Unique changes were observed for DNA-SWCNTs hybrids upon surfactant exchange, including distinct reaction time constants ranging from 9 s to 230 s and an increase in photoluminescence ranging from 1.3 to 14.7-fold. Additionally, DNA-wrapped SWCNTs showed unique interaction behavior and stability in cell culture medium. The CTC_3TC-(7,6) hybrid exhibited the largest time constant upon surfactant-exchange and was the only hybrid to show an increase in near-infrared (NIR) fluorescence intensity in serum-containing cell culture medium. Moreover, we explored covalent functionalization of chirality-pure SWCNTs via oxygen doping and oriented immobilization of disaccharide lactose-containing glycopolymers. We observed a strong dependence on oxygen doping on surface-coatings of nanotubes

when exposing various aqueous dispersions of SWCNTs to short wavelength ultraviolet (UV) light. Our results provide a foundation for future development of applications for chirality-pure SWCNTs in biochemical sensing and imaging advancement. Successful completion of the covalent functionalization of SWCNTs with lactose-containing glycopolymers will lead to the creation of engineered multicolor, fluorescent probes with precise optical and carbohydrate functionalities. These fluorescent probes will serve as a novel nanomaterial tool to enable better understanding of the carbohydrate-protein interactions in biology.

TABLE OF CONTENTS

Page

LIST OF TABLES

LIST OF FIGURES

CHAPTER I

INTRODUCTION

Single-wall carbon nanotubes (SWCNTs) are excellent candidates for many applications including bioimaging, biosensors, and drug delivery [1–5] as they are low dimensional nanomaterials that possess unique physical, electronic, chemical, and optical properties.[6–10] For many years, researchers have utilized SWCNTs as multifunctional optical probes [11,12] due to their well-defined electronic structures and optical properties, particularly the intrinsic photoluminescence (PL) in the tissue transparent near-infrared (NIR) spectral regime[13–15]. In addition, SWCNTs have vast potential for surface modification, including covalent and noncovalent methods, because all their atoms comprise a surface. For instance, SWCNTs have been used as basis for nanodevices for selective sensing and imaging due to their high aspect ratio, thereby allowing attachment of molecules for molecular recognition.[16–19] For many applications, a SWCNTs of specific chiral structure is desired, in which case purification of chirality-pure SWCNTs is crucial. Many advances have been made regarding nanotube sorting and separation of single-chirality SWCNTs in aqueous solutions via surface modification. Specifically, SWCNTs can be non-covalently functionalized with single-stranded DNA (ssDNA) to efficiently separate single-chirality SWCNTs from a synthetic

mixture. Due to their preserved intrinsic properties from non-covalent method, SWCNTs wrapped with recognition sequences of ssDNA have been utilized in many *in vivo* and *in vitro* applications for biological detection, imaging, and therapeutics.[2,4] Chirality-pure SWCNTs allow for a less cytotoxic and a more controlled method of drug delivery[2,20], compared to using an as-synthesized SWCNT mixture.

Furthermore, the NIR photoluminescence of SWCNTs can be chemically tuned with molecular precision by utilizing chirality-pure SWCNTs as nanomaterial hosts for engineered organic color centers.[21] The tunable NIR optical functionality of SWNCTs has applications in biosensing and imaging as well as telecommunications, optoelectronics and photonics due to their capability to behave as single photon emitters at room temperature.[7,8–10] Here, the covalent functionalization allows for tunability and control of desired properties through covalent attachment of numerous functional groups that permanently alter the SWCNT surface structure. This can be done through oxygen doping or creation of sp^3 defects on the nanotube surface using functional groups, such as diazonium salts[25–27] and organic groups.[28] Recently, oxygen-doped SWCNTs created by reacting with ozone[29] and bleach_ were utilized as fluorescent probes for *in vivo* imaging in mice using NIR spectroscopy.

In this thesis, we report the elucidation of the complexation of chirality-pure SWCNTs with the recognition ssDNA sequence on ten different chirality-pure (*n,m*) SWCNTs. The DNA conformation as well as its binding affinity to SWCNTs has been investigated by many researchers, using experimental techniques including fluorescence and absorption spectroscopy, [31–33] and through molecular dynamics simulations, [34–37] and machine learning.[38] Here, we used sodium deoxycholate (SDC), a strong

surfactant that is known to displace DNA from nanotube surface, to elucidate the binding of DNA to SWCNTs by measuring NIR fluorescence. Nanotube emission intensity is highly sensitive to small environmental changes, resulting in emission intensity changes as well as spectral wavelength shifts, allowing for a fast and efficient method to investigate the DNA-surfactant exchange reaction. Additionally, absorption and PL spectroscopy were utilized to investigate the stability of each of these DNA-SWCNT hybrids in cell culture media with and without fetal bovine serum (FBS), as stability of SWCNTs in biological environments is a prerequisite for many biological applications.

Moreover, we report work on covalent functionalization of chirality-pure SWCNTs using glycopolymers with chain-end light-activatable phenyl azide moiety as well as using oxygen doping. Synthetic glycopolymers have been explored in functionalization of nanomaterials and have been utilized in biosensing applications.[39] Successful completion of this work can lead to the design of a multifunctional SWCNT hybrid with applications in profiling carbohydrate-protein recognitions, particularly for carbohydrate-binding proteins. Furthermore, the optical properties of pristine SWCNTs can be tuned due to the creation of sp^3 defects from the covalent attachment of the aryl azide functional group to the nanotube surface. In addition, a doping effect from oxygen dissolved in solvents was observed when simply exposing SWCNT samples under ultraviolet (UV) light. This simple oxygen doping phenomenon was investigated using different molecular coatings on the nanotube surface, as well as using different SWCNT chirality species.

1.1. Thesis Outline

This thesis is formatted into two main sections: the first section includes the published paper on non-covalent modification and the second section includes work on covalent chemistry of SWCNTs. Specifically, chapter 2 includes background on carbon nanotubes and other relevant information. In chapter 3, is the published paper on chirality-pure SWCNTs wrapped with ssDNA. The kinetics of the binding affinity of a recognition sequence DNA with a pure-chirality SWCNT was investigated through surfactant exchange of DNA with SDC. This interaction was characterized via absorbance and fluorescence spectroscopy. We also studied the stability and interaction mechanism of ssDNA-SWCNT hybrids in cell culture media with and without fetal bovine serum. Chapter 4 includes the introduction to covalent functionalization of SWCNTs. Chapter 5 provides the experimental details for covalent functionalization as well as glycopolymer synthesis. Chapter 6 follows with work performed on covalent functionalization with glycopolymers as well as oxygen doping. The thesis is concluded in chapter 7 with summary of major finding as well as a discussion of the future directions for the work.

CHAPTER II

BACKGROUND

The unprecedented interest in carbon nanotubes began with the observation of carbon nanotubes by Iijima in 1991.[40] Shortly thereafter, in 1993, Iijima and Ichihashi along with Bethune et al., independently discovered single-wall carbon nanotubes (SWCNTs).[27,28] Later, in 1995, Smalley and co-workers at Rice University developed a process to synthesize SWCNTs,[42] enabling subsequent studies and breakthroughs on SWCNTs for the next two decades. Expanding upon that work, various methods have been developed to achieve synthetic SWCNTs including catalytic chemical vapor deposition (CVD)[43] and high-pressure carbon monoxide (HiPco).[44,45] CoMoCAT is a commonly known process to synthesize SWCNTs, that uses Cobalt (Co) and molybdenum (Mo) as catalysts.[46] These production techniques can produce quantities up to several grams of SWCNTs per hour. SWCNTs synthesized through these methods are polydisperse in length, are variable in electronic character and contain a variety of impurities including metallic catalyst particles and amorphous carbon.[43] These impurities, as well as the lack of structural control, inhibit the effective utilization of unique properties of SWCNTs, and consequently, hinder application in device

fabrication. As such, in order to understand their properties as well as facilitate structure control, purification of as-synthesized SWCNTs is a critical step, especially concerning biological applications. Most commonly, commercially available SWCNTs are sold as powders and nanotubes are not soluble as individuals in water or any other solvents (superacids are the exception[47,48]) due to the strong van der Waals attraction between SWCNTs (≈0.5 eV/nm)[49] and the highly amphiphobic nature.[49] In order to disperse nanotubes, a dispersant that can adsorb to the nanotube surface, such as short single-stranded DNA (ssDNA), needs to be added to overcome the van der Waals forces and stabilize individually dispersed SWCNTs in liquid media. A stable dispersion allows for further liquid phase processing, such as purification steps for producing chirality-pure SWCNTs and enabling surface modification via solvent filling or chemical functionalization. Extensive amount of work has been conducted in nanotube sorting and separation of various nanotube species from a synthetic mixture. This is particularly important in developing SWCNTs applications for electronic devices as well as for bioimaging and sensing applications.

2.1. Carbon Nanotubes

Carbon nanotubes (CNTs) are one-dimensional allotropes of carbon nanomaterials with hollow, cylindrical nanostructures of carbon atoms that are sp^2 hybridized. They have diameters d of $\approx$ 1 nm and lengths L up to several millimeters, with aspect ratios L/d up to ≈100,000. There are two main types of CNTs: multi-wall carbon nanotubes (MWNTs) which are composed of multiple concentric tubes and SWCNTs. Essentially, SWCNTs can be envisioned as a single graphene sheet rolled into a cylinder (Figure 2.1.). Each carbon atom is covalently bonded to three neighboring

carbon atoms via σ-bonds, and the remaining p-electrons of each carbon atom form an extended π-electron system.[50] The SWCNT structure is specified by the vectors $\mathbf{C_h}$ and **T**, where $\mathbf{C_h}$ is the chiral (or roll-up) vector and **T** is the translational vector. The length of $C_h = na_1 + ma_2$ defines the CNT circumference, where $a_1$and a_2 are the base vectors of the graphene sheet and (*n, m*) is the chiral index by which each carbon nanotube is identified. The different geometries arise from the differences in the chiral index and the chiral angle θ of SWCNTs. For instance, $m = 0$ corresponds to zigzag nanotubes, and $n = m$ corresponds to armchair nanotubes. All other (*n, m*) species designate chiral nanotubes.

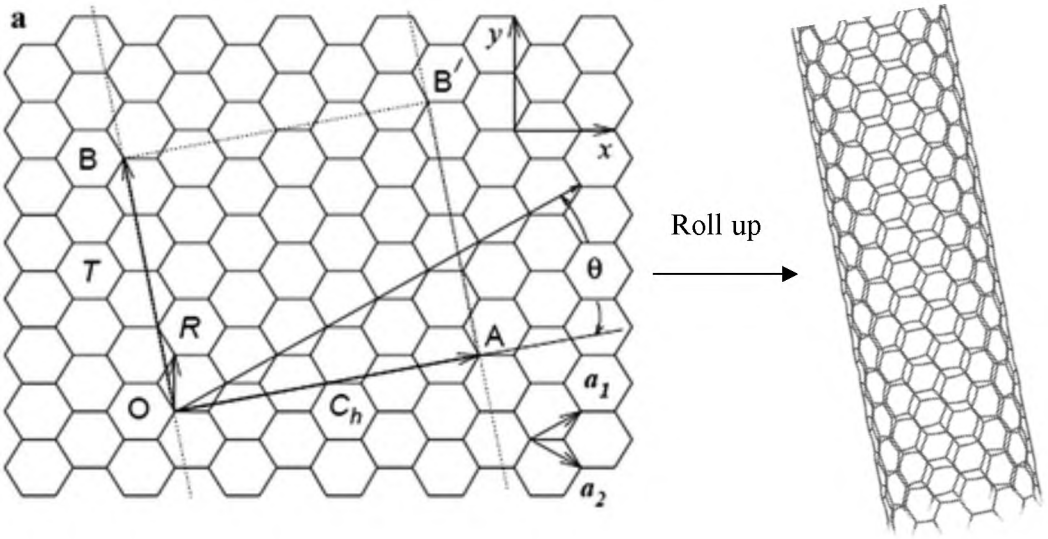

Figure 2.1. Representative graphene sheet with corresponding vectors, and an atomic depiction of a nanotube (rolled-up graphene sheet). (Reproduced from Ref[51])

The (*n, m*) chiral structures of SWCNTs define their unique electronic properties as well. Specifically, each nanotube with a corresponding pair of integers (*n, m*), has a well-defined diameter and chiral angle, which defines their optical and electronic properties. For instance, armchair SWCNTs (i.e., $n = m$) are metallic tubes while zigzag (i.e., $m = 0$) and chiral (i.e., $n \neq m$) SWCNTs can be either quasi-metallic [i.e., mod

$(n-m,3)=0$) or semiconducting tubes [i.e., mod $(n-m,3)=1\ or\ 2$].The chiral angle θ for chiral (*n, m*) SWCNTs is between 0° to 30° whereas for armchair and zigzag SWCNTs is 0° and 30°, respectively. Examples of specific (*n, m*) SWCNT species of three electronic types are shown in Figure 2.2. Additionally, chiral (*n, m*) SWCNTs can be left-handed and right-handed enantiomers that are essentially mirror images (Figure 2.3).

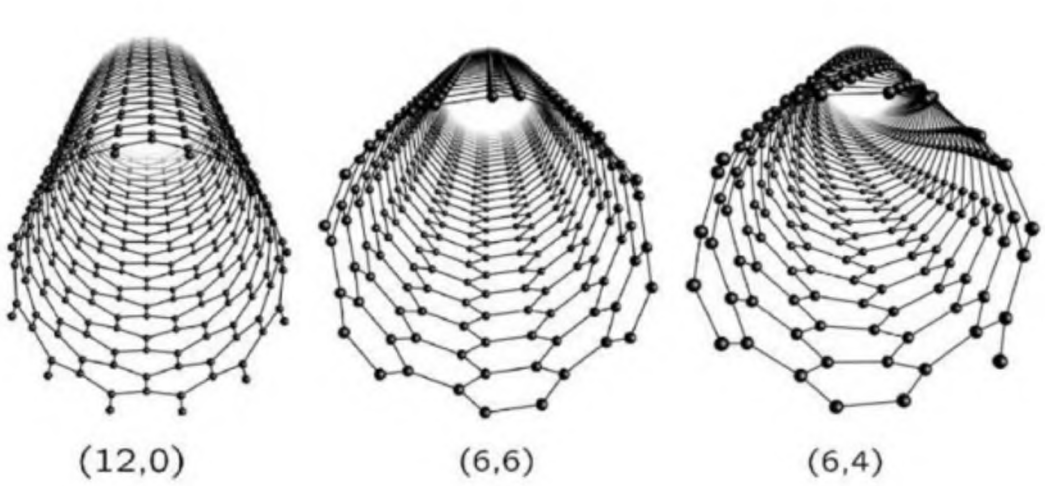

Figure 2.2. Three electronic structures of SWCNTs: zigzag (12,0), armchair (6,6), and chiral (6,4). (Reproduced from Ref[52])

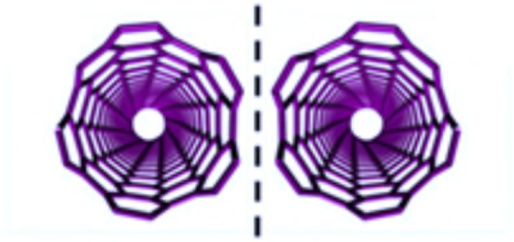

Figure 2.3. (6,5) enantiomers. (Reproduced from Ref[53])

In terms of physical properties, both experimental and theoretical studies have shown that the Young's modulus of SWCNTs is around 1TPa[1] (five times greater than

steel) and tensile strength reaches up to 52 GPa[55], and they are known to be stable up to ≈ 450°C in air[56] making them intriguing for many applications. Here, we focused on the optical properties and surface modification of pure-chirality semiconducting SWCNTs due to their intrinsic near-infrared (NIR) fluorescence, particularly for developing biomedical applications.

Various methods of synthesizing SWCNTs, including HiPco and CoMoCAT result in polydispersity in atomic structures and physical dimensions. Although it is impossible to produce a singular specific type of carbon nanotubes, there are techniques that can produce semiconducting nanotubes enriched synthetic powders. Semiconducting SWCNTs are the focus of this work and are particularly interesting as they emit in the NIR region, where biological tissues have low autofluorescence[3,57,58]. The optical properties of SWCNTs can be characterized via vis-NIR absorption, NIR photoluminescence (PL), and Raman scattering. Photon emission is primarily due to the electron-hole bound state known as excitons.[8,59] Covalent functionalization of SWCNTs relies on changes to the excited state of these excitons[23,24,26,60] (described in more details in the **2.4. Covalent Functionalization** subsection).

2.2. DNA-Wrapped SWCNT Hybrids

As mentioned previously, single-stranded deoxyribonucleic acid (ssDNA) is a biopolymer that can disperse SWCNTs individually in a solvent. DNA is composed from four nucleotide bases and a negatively charged backbone of phosphate and sugar groups. ssDNA can be synthesized with lengths up to 100 nucleotides with high purity and yield. Effective dispersion and separation of SWCNTs in water aided by ssDNA was first shown by Zheng et al.[61,62] DNA is a biomolecule that can go through conformational

changes depending on the solvent environment. Tu et al. proposed that ssDNA folds in an ordered structure around the nanotube surface (Figure 2.4).[63] Its hydrophobic nucleotide bases noncovalently interacts with the hydrophobic nanotube surface via $\pi - \pi$ stacking while its hydrophilic phosphate-sugar backbone stabilizes the hybrids through electrostatic interactions , allowing SWCNTs to remain individually dispersed in aqueous environments.

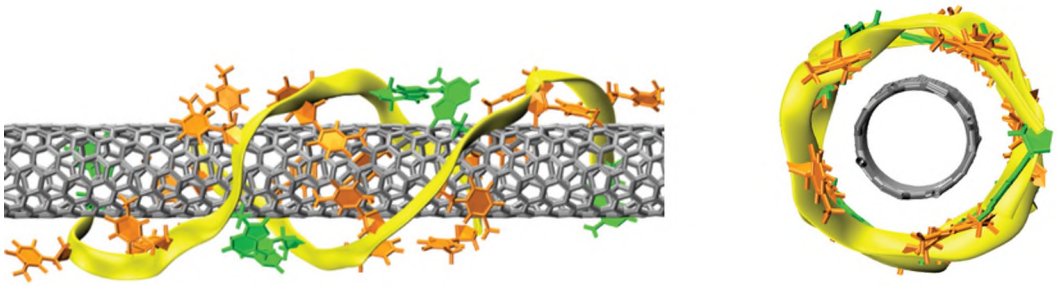

Figure 2.4. Wrapping of a DNA strand on the nanotube surface. (Reproduced from Ref[63])

Additionally, it has been shown that the ordered wrapping structures of ssDNA on the SWCNT surface is strongly sequence dependent[64] leading to the selection of recognition DNA sequences for specific (*n, m*) SWCNT species.[65] Extensive research on ssDNA-SWCNTs has led to separation and sorting of nanotubes with defined handedness and helicity control, for nanotubes of different chirality and all three electronic types. A recognition ssDNA-SWCNT pair has a distinct hydration energy that is different from nonrecognition ssDNA-SWCNT hybrids in the dispersion. This allows for the selective separation of a pure-chirality ssDNA-SWCNT hybrid in a polymer aqueous two-phase (ATP) system depending on the affinity of DNA-coated SWCNTs for each water phase.[66]

DNA being a biomolecule, improves the biocompatibility of these DNA-SWCNT hybrids for biological applications, and promotes the interest in further understanding the stability and properties of these hybrids in various solvent environments.

2.3. DNA-Surfactant Exchange Reaction and Characterization by Optical Spectroscopy

Optical spectroscopy, the study of absorption or emission of light, can offer precise insights into a material's electronic structures, and is of particular interest when studying nanomaterials. The quasi one-dimensional SWCNTs exhibit van Hove singularities that govern the optical absorption and emission features of SWCNTs.[67] Chirality-pure (*n, m*) SWCNTs have clearly identifiable optical transition peaks such as E_{11}, E_{22}, and E_{33} in a broad spectral regime from UV to visible to NIR wavelengths (Figure 1 and 2 in Appendix A). Particularly, the lowest-lying electronic state corresponds to the E_{11} transition peak in the NIR. Distinct SWCNT species exhibit high optical anisotropy ,[68] which makes optical spectroscopy a useful technique to study the optical properties of SWCNTs.

Surfactants are molecules that are known to disperse nanotubes. As such, they are also one of the methods used by various researchers to elucidate the binding affinity of DNA to carbon nanotube surfaces, mainly on synthetic mixtures of CNTs. The transition energies of SWCNTs, particularly the E_{11} transition peak, are sensitive to the solvent environment as well as adsorbed molecules[67,69–71] that modulate the local dielectric properties surrounding nanotubes. Thus, spectral changes of electronic transitions occur in the forms of solvatochromic shifts (i.e., spectral shift) as well as changes in spectral width and intensity when adsorbed molecules are replaced by another. For instance, when

DNA strands are displaced by a surfactant molecule, a blue shift of E_{11} peak (i.e., decrease in wavelength) is observed. Different coating molecules, nanotube surface coverage, and solvents will modulate the E_{11} transitions peaks of SWCNTs. Given the particularly sensitive nature of SWCNT fluorescence to the surrounding environment, measuring the absorption and fluorescence spectroscopy of SWCNTs with well-defined structures is an effective method to study DNA displacement by a surfactant.

2.4. Covalent Functionalization

Surface functionalization of carbon nanotubes is essential as it enables the suspension of individualized carbon nanotubes in solvents. The ssDNA method described above, as well as the wrapping of nanotubes by surfactants[68,72–74] and polymers[17,75,76], fall into the category of noncovalent complexation for SWCNTs. Another method that can be used to individually disperse nanotubes as well as enable tailoring of their properties is covalent functionalization. Mickelson and coworkers were the first to achieve covalent functionalization of CNTs by treating them with elemental fluorine.[77] Since then, the field of covalent functionalization of SWCNTs has been vastly explored by many researchers. Noncovalent methods leave the sp^2 carbon lattice intact with very little disruptions and protects the intrinsic properties of nanotubes. In contrast to that, covalent functionalization changes the hybridization of the carbon atoms from sp^2 to sp^3 due to the covalent binding of specific functional groups to the nanotube surface. Consequently, the creation of these "defect" sites on the nanotube surface changes the structural and optical properties of CNTs, enabling their potential use in various applications.

As mentioned briefly prior, the optical properties of nanotubes arise from excitons, (electron-hole pairs bound by Coulomb interactions).[78,79] In semiconducting SWCNTs, excitons move continuously along the nanotube axis.[8,80] As excitons return to their ground state, they can emit a photon (photoluminescence). The radiative lifetime of these excitons can be uncertain. Depending on the solvent and therefore dispersion quality, the excitons go through a nonradiative decay. Coating molecules including DNA and surfactants, can suppress this nonradiative decay, by shielding excitons from the solvent environment.

Covalent functionalization converts the sp^2 carbon lattice to a sp^3, breaking the symmetry, and create a local energy minimum (Figure 2.5.). This local energy minimum lies below the original E_{11}, creating a new, optically allowed state that allows "dark" state excitons to emit light.[25] The introduced sp^3 defects serve as a trap site for mobile excitons in which excitons can relax to their ground state and emit a photon. The trapped excitons are shielded from the nonradiative quenching sites generated from charge transfer and Fermi level shifts[81] on the nanotube surface (Figure 2.6.). Consequently, excitons can fluoresce more brightly and at longer wavelengths in the NIR region (> 1100 nm). The NIR region beyond 1100 nm is of high interest for biological imaging applications as biological materials have very weak background photoluminescence (PL).

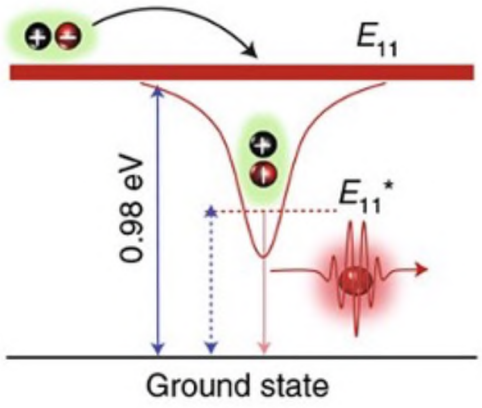

Figure 2.5. Trap states created below the original E_{11}, in which excitons are trapped. (Reproduced from Ref[24])

Through the sp^3 defect, a new PL peak arises at this lower energy state, known as E_{11}^- (or E_{11}^*), due to the radiative recombination of the trapped excitons. The ultimate goal of utilizing covalent attachment for optical property enhancement, is to produce this E_{11}^- peak where nanotubes fluoresce much brighter than the original E_{11} peak and have a longer lifetime than is found with pristine SWCNTs.

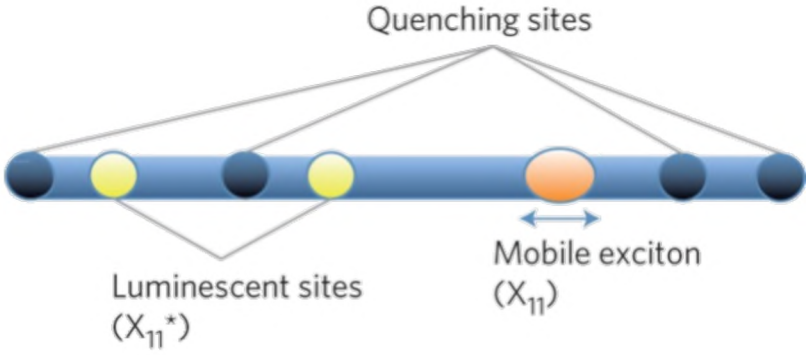

Figure 2.6. Schematic of exciton mobility on a nanotube surface including local luminescent and quenching sites. (Reproduced from Ref[23])

Additionally, the covalent attachment (i.e., formation of a carbon–functional group bond) can be observed through Raman spectroscopy. Specifically, a Raman D band

(~1300 cm^{-1}), corresponding to nanotube surface defects, arises when the new covalent bond is formed.[67] Covalent attachment to the nanotube surface has been successfully employed in surfactant-coated SWCNTs via diazonium reactions.[25,26] Covalently modified SWCNTs allow for tuning of the emission intensity, essentially turning SWCNTs into organic color centers.[21] Many researchers in the recent years, have shown promising results in the field of covalently functionalized SWCNTs and have even utilized SWCNTs with the new E_{11}^{-} peak as optical sensors for *in vivo* applications.[29,30]

2.4.1. Glycopolymers

The interest of this work includes the tailoring of SWCNT surface with glycopolymers. Glycans are major determinants of molecular recognition on the cell surface including diverse processes such as cell signaling, cell trafficking, and endocytosis.[82] It has been demonstrated that glycopolymers that mimic cell surface mucin glycoproteins can coat CNTs,[39,76] and functionalize other nanomaterials.[83,84] These types of glycopolymers have also found application as biosensors and in drug delivery.[84,85] In this work, biomimetic glycopolymers with a chain-end functionalized aryl (phenyl) azide ($-N_3$) group were used to explore the covalent functionalization of SWCNTs. Theoretically, as shown on previous studies of phenyl azide photoactivation, when exposed to short wavelength UV light (254 nm, 265 to 275 nm[86]), $-N_3$ forms radicals, particularly the highly active nitrene,[87–89] that enable covalent attachment to C=C bonds in SWCNTs. Consequently, yielding SWNCT-hosted organic color centers with oriented and immobilized glycopolymer.

2.4.2. Oxygen doping

Covalent modification can also be in a form that does not result in sp^3 hybridization of carbons. This can be achieved via oxygen doping. Under UV light exposure, excited oxygen singlet molecules, denoted as $^1O_2$,[90,91] can attach to the SWCNT surface, essentially creating a defect site that serves the same purpose as the sp^3 defect described prior. This permanent covalent attachment of oxygen to the SWCNT surface is different than the oxidizing effect of oxygen on SWCNTs which quenches the nanotube emission intensity.[92]

CHAPTER III

This chapter is a reprint of the paper, "Chirality-pure carbon nanotubes show distinct complexation with recognition DNA sequences", published in *Carbon* **2020**, 167, 601-608.

Chirality-Pure Carbon Nanotubes Show Distinct Complexation with Recognition DNA Sequences

Abstract

Pure-chirality single-wall carbon nanotubes (SWCNTs) that are non-covalently complexed with recognition DNA sequences exhibit unique interaction behavior and hybrid stability in aqueous environments. The complexation of DNA-wrapped SWCNTs was found to be a strong function of both the DNA sequence and SWCNT chiral structure, highlighted by the distinct coating displacement of the same recognition DNA sequence from a pair of (6,5) enantiomers by a strong surfactant. A broad range of changes were observed for different DNA/SWCNT recognition pairs with surfactant exchange including the increase in nanotube photoluminescence intensity in the near-infrared (NIR) from 1.3 to 14.7-fold and time constants deduced from DNA displacement kinetics ranging from 9 s to 230 s. A large time constant of 230 s and a relatively small

4.4-fold increase in NIR emission intensity were obtained for the CTC_3TC-(7,6) hybrid highlighting the vast potential of short DNA sequences for improved nanotube sorting and hybrid stability in aqueous environments. Additionally, CTC_3TC-(7,6) was identified as the only hybrid to exhibit an increase in NIR fluorescence intensity in serum-containing cell culture media among all samples tested. Our results demonstrated unique optical properties and hybrid stability of DNA/SWCNT recognition pairs, providing a foundation for developing applications of chirality-pure SWCNTs.

3.1. Introduction

Single-wall carbon nanotubes (SWCNTs) are multifunctional nanomaterials with exceptional optical, electronic, mechanical, and chemical properties and have been the subject of extensive studies involving both *in vitro* and *in vivo* interactions with chemicals [16,17,72,93] and biomolecules [4,12,18,94,95]. Recent advances in post-synthesis sorting of carbon nanotubes, such as the use of recognition sequences of single-stranded DNA (ssDNA) to effectively select pure-chirality SWCNT species with a defined chiral index (*n, m*), have provided a material foundation for creating new nanomaterial tools with well-defined properties for biological imaging, sensing, and therapeutic applications [1,4,64,65,96,97]. The highly predictable electronic structures and optical properties of chirality-defined SWCNTs, such as the distinct E_{11} electronic transition of nanotubes, offer many advantages for biochemical sensing and imaging advancement [68]. Particularly, semiconducting SWCNTs fluoresce exclusively in the near-infrared (NIR) region between approximately 900 to 1600 nm, that has attenuated autofluorescence and deep tissue penetration, providing the ideal condition for high contrast fluorescence detection in biological media [3,13–15]. Pure-chirality SWCNTs

can be further utilized as spectrally coded, multicolor fluorescent probes that can selectively and sensitively detect analytes in many applications, such as targeted sensing, ratiometric sensors, and multiplexed imaging [3,13,98,99]. In addition, pure-chirality SWCNTs promote advances in ultra-low dose, high efficiency nanomedicines showing more than ten-fold lower dose compared to that of as-synthesized SWCNT mixtures when utilized as a multifunctional imaging, sensing, and therapeutic agent [2,4]. More recently, pure-chirality SWCNTs have been demonstrated as promising nanomaterial hosts for organic color centers, an emerging class of synthetic quantum emitters with robust, tunable NIR optical functionality for advanced technological applications in biosensing and bioimaging, optoelectronics, and photonics [21,24,30,100].

In addition to offering a powerful method for selecting specific (*n, m*) species in polymer aqueous two-phase (ATP) systems [38,65,66,101], DNA-wrapped SWCNT hybrids (DNA-SWCNTs) formed by non-covalent complexation through multivalent π–π interactions [102] between the DNA bases and the nanotube surface have demonstrated many interesting properties. These include selective modulation of the nanotube PL [92,103], targeted detection of biomolecules and biological processes [4,5,99], and enhanced biocompatibility and stability in intracellular environments [20,104] that are highly dependent on the combination of DNA sequence and SWCNT chirality. The underlying structural basis for sequence-dependent properties of DNA-SWCNTs has been linked to the formation of ordered DNA wrapping structures on the nanotube surface providing unique surface functionalities for each purified hybrid [34,37,105]. The distinct binding of a DNA recognition sequence towards a specific (*n, m*) species, including enantiomers of a (*n, m*) SWCNT, can lead to a small difference in the solvation

free energy of the hybrid, yet sufficient to differentiate the selected hybrid from a nanotube mixture in a ATP system that has slightly different physical properties [34,35,65,101].

The DNA binding to SWCNTs have been determined by many techniques through measuring interaction forces and thermodynamics of the hybrid to understand the unique structural and physical properties of DNA-SWCNTs. These include AFM studies of peeling DNA oligomers from nanotube [106], fluorescence spectroscopy of DNA-SWCNTs upon reactions with O_2 and surfactants [70,92,107,108], absorption spectroscopy of DNA-SWCNTs with surfactant exchange [31–33], and molecular dynamics simulations [34–37] and machine learning [38] approaches to elucidate and even predict the DNA coating structure on a nanotube. Among these techniques, kinetics of the DNA displacement by a surfactant through monitoring fluorescence spectral changes have been proven to be a fast and efficient way to probe the complexation affinity of a DNA sequence and SWCNT chirality. This is due to the highly sensitive nanotube PL as compared to its absorption, allowing detection of small perturbations in the external environment through measuring spectral changes of sharp emission peaks of (*n, m*) SWCNT in the NIR [70,107,108]. However, previous studies on kinetics of surfactant exchange of DNA coatings have been limited to either a synthetic SWCNT mixture comprised of a population of over thirty different (*n, m*) SWCNT species or a (6,5)-enriched SWCNTs complexed with a non-recognition ssDNA sequence. Although the binding affinities between ssDNA and SWCNTs have been quantitatively deduced in these studies, the interference of many (*n, m*) SWCNT species within a polydisperse molecular system and the random combination of DNA/SWCNT may diminish efforts in

elucidating distinct interactions of DNA-SWCNT recognition pairs that yield unique optical and physicochemical properties for applications.

Here, we report the first comprehensive work on elucidating the distinct complexation of chirality-pure SWCNT and recognition ssDNA sequence by NIR fluorescence spectroscopy through measuring the DNA coating displacement by sodium deoxycholate (SDC), a surfactant known to bind strongly to nanotubes. A total of ten pure-chirality semiconducting (*n, m*) SWCNT species, including a pair of (±) (6,5) enantiomers, have been purified by our previously reported method using recognition DNA sequences in polymer ATP systems [65,66]. The polymer ATP separation method allows us to purify sufficient quantities of nanotubes and perform a minimum of three repeats of each experiment described in this work. The spectral modulation of pure chirality (*n, m*) SWCNTs including spectral wavelength shifts and changes in spectral line width and emission intensity were monitored in aqueous environments. We treated kinetics of DNA displacement with single-exponential fits to changes in fluorescence emission intensity as a function of time upon surfactant exchange. Characteristic optical features, such as PL intensity increase and deduced time constants with surfactant exchange, were found to be unique to each DNA-SWCNT hybrid with no clear dependence on the DNA length and nanotube diameter. The role of (*n, m*) chiral structure on the DNA binding was further highlighted by displacing the same recognition DNA sequence from a pair of (6,5) enantiomers. In addition, changes in absorption and emission intensities of pure-chirality SWCNT species have been monitored in both serum-free and fetal bovine serum (FBS)-containing cell culture media. Purified DNA-SWCNTs showed relatively stable spectral features in serum-containing cell culture

media than those exposed to serum-free media, providing potential of creating NIR optical probes with improved stability and specific functionality for biological applications. These findings provide better understandings of distinct complexation of DNA/SWCNT recognition pairs, offering important insights for developing effective nanotube sorting and stable optical nanoprobes for biochemical sensing and imaging applications utilizing pure-chirality SWCNTs. Representative spectroscopy findings are presented in the main text, but a substantial amount of experimental data is also included in the Supplementary Data.

3.2. Experimental Section

3.2.1. Preparation of pure-chirality (n, m) SWCNT species by DNA

Stock DNA-SWCNT dispersions and pure-chirality (*n, m*) species were prepared according to the previously published procedure [65,109]. Briefly, CoMoCAT SWCNT powders (SG65i-L39 and EG150-L670; CHASM Advanced Materials) were dispersed in a total volume of 1 mL aqueous solutions of recognition DNA sequences (Integrated DNA Technologies) containing 0.1 mol/L NaCl by tip sonication (model VCX 130, Sonics and Materials, Inc.) in an ice bath for 2 hours at a power level of 8 W. The SWCNT/DNA mass ratio was 1:2 with a fixed SWCNT concentration of 1 mg/mL. Supernatant dispersions were collected after 90 min centrifugation at 17,000 g for SWCNT purification. A total of ten (*n, m*) species including (7,3), (±) (6,5) enantiomers, (9,1), (8,3), (8,4), (7,6), (9,4), (11,1) and (10,3) were isolated in polymer aqueous two-phase (ATP) systems including 7.76 mass% poly(ethylene glycol) (6 kDa)/15.0 mass% polyacrylamide (10 kDa) (PEG/PAM) and 5.50 mass% PEG/7.50 mass% dextran (70 kDa) (PEG/DX) (Figure 1 and 2 in Appendix A.) [65]. The selection of recognition

DNA sequences and details of SWCNT separation can be found in prior work.[65,66] Purified SWCNT species have diameters ranging from 0.706 to 0.936 nm [68] and an estimated number average length of 350 ± 100 nm [65]. Each (*n* ,*m*) species is enriched in one of the handedness for chiral tubes, with (±) (6,5) tubes having the enantiomeric excess of > 90% for each handedness tube based on our previous report [65]. Here, the plus or minus sign of (6,5) species is assigned according to the signs of the circular dichroism values at the E_{22} position of (6,5) near 573 nm.

Polymers were removed according to the SWCNT precipitation method reported previously [65,109,110]. Briefly, a final concentration of 0.5 to 1.0 mol/L sodium thiocyanate (NaSCN, Sigma-Aldrich) was added to purified (*n, m*) SWCNT species in polymer phases, and the sample was incubated overnight at 4 °C. Adding the corresponding DNA recognition sequence at 100 μg/mL during the incubation stage is recommended to prevent nanotube aggregation. Then, the mixture was centrifuged at 17,000 g for 30 min to remove the solvent and the purified (*n, m*) SWCNT pellet was resuspended in deionized (DI) water by bath sonication at room temperature for 30 min. The corresponding DNA sequence at a final concentration of 100 μg/mL was added to purified SWCNT species to improve the dispersion stability for a long-term storage.

3.2.2. Displacing DNA coatings of nanotubes by a surfactant

A stock solution of 10 mass % sodium deoxycholate (SDC) (98 %, BioXtra) was prepared for DNA/surfactant replacement experiment at room temperature. The concentration of purified (*n, m*) SWCNT species was adjusted to an absorbance of 0.3 ± 0.02 at its E_{11} peak wavelength for surfactant exchange experiment, which corresponds to approximately a nanotube concentration of 1.65 μg/mL [111]. The complexation

affinities of purified DNA-SWCNT hybrids in aqueous surfactant solutions were examined by three repeats using a total volume of 120 μL for each nanotube sample. Roughly 5 s after the initial measurement of DNA-SWCNT fluorescence, small aliquot of 0.6 μL stock SDC solution were added to DNA-SWCNT samples and mixed immediately to obtain a final concentration of 0.05 mass % SDC.

3.2.3. Incubation of purified DNA-SWCNTs in cell culture media

Purified (*n, m*) SWCNT species were incubated in Gibco™ RPMI 1640 Medium (Catalog No. 11-875-085, FisherScientific) containing 10 % (v/v) fetal bovine serum (FBS, Corning) at pH 7.54 for up to 8 hours in dark at room temperature, unless indicated otherwise, to monitor the dispersion stability of purified DNA-SWCNT hybrids in cell culture media. Cell culture medium without FBS showed pH 8.3-8.4 during the 8 hour incubation. The optical spectroscopy of purified DNA-SWCNT hybrids in cell culture media was examined by three repeats. Small aliquots of 1-4 μL of concentrated, purified SWCNT samples were added to a total volume of 120 μL cell culture media with and without serum to obtain an absorbance value of 0.3 ± 0.02 at the E_{11} peak wavelength of SWCNTs (i.e., approximately 1.65 μg/mL tubes).

3.2.4. Optical characterization of purified DNA-SWCNTs

Spectroscopy characterization including vis-NIR absorbance and near-infrared (NIR) fluorescence measurements were performed on a NS3 NanoSpectralyzer (Applied NanoFluorescence, LLC) using a 10 mm path length quartz cuvette. Fixed excitation wavelengths of 532 and 641 nm lasers, corresponding to E_{22} peak positions of (*n, m*) species, were used for acquiring NIR fluorescence spectra. DNA displacement kinetics were monitored using sequence mode data acquisition through time-resolved

fluorescence spectra at room temperature at a final concentration of 0.05 mass % SDC. MATLAB R2018b software was used for exponential fitting of DNA displacement kinetics.

3.3. Results and Discussion

3.3.1. Preparation and optical characterization of DNA/surfactant exchange for pure-chirality SWCNTs

The structural diversity of SWCNTs produces a family of cylindrical carbon allotropes, where each (*n, m*) species exhibits unique optical and physicochemical properties for a wide range of applications, such as biochemical sensing and imaging. Separation of a pure-chirality (*n, m*) SWCNT with well-defined diameter, chiral angle, and electronic structure from their synthetic mixture is generally considered as a prerequisite for many applications. We isolated a total of ten pure-chirality (*n, m*) species using recognition DNA sequences by a polymer ATP separation method [65]. The corresponding absorbance and fluorescence spectra of purified DNA-SWCNTs clearly showed optical transition peaks of (*n, m*) species, such as E_{11} and E_{22} with little to no contribution from any other species (Figures 1 and 2, Appendix A.). In addition to providing a source of chirality-pure nanotubes, purified DNA-SWCNT hybrids with ordered DNA folding structures exhibit vast potential as stable, biocompatible fluorescent probes to detect targeted biological interactions in the NIR [4]. It is important to utilize pure-chirality SWCNTs, as opposed to a synthetic SWCNT mixture, to study fundamental interaction behaviors of DNA/SWCNT recognition pairs. The interaction behavior of non-recognition DNA sequences with SWCNTs is not within the scope of this work.

The recognition DNA sequence forms an ordered wrapping structure in a single layer along the specific (*n, m*) SWCNT, creating different DNA coverages on the surface of nanotube (i.e., relating to the DNA density on tubes). However, the difference in the DNA coverage should not affect the complexation of recognition pairs of DNA and SWCNT investigated by DNA/surfactant exchange [108]. We displace DNA coatings on a purified (*n, m*) species by adding a final concentration of 0.05 % SDC and directly measure spectral changes of both absorbance and fluorescence of nanotube samples at equilibrium (Figure 3.1.). The concentrations of SDC and nanotubes used give a mass ratio of ≈ 300:1 for SDC: (*n, m*) SWCNT, leading to the full displacement of DNA by excess SDC [31]. The absorbance spectra of nanotube samples showed varied spectral shifts (< 9 nm) to shorter wavelengths at the E_{11} peak of different (*n, m*) species, which is expected when displacing DNA with a strong surfactant (Table 1, Appendix A.). Absorbance values at E_{11} remained relatively stable upon complete DNA displacement by SDC at equilibrium, an example of which is shown for $CTTC_3TTC$-(9,4) hybrid (Figure 3.1.b.). In comparison, spectral variations in nanotube emission after surfactant exchange, including intensity increase, narrowing of line width, and blue shift (i.e., decrease in wavelength) of the E_{11} peak of (*n, m*) species, showed large differences for different recognition pairs of DNA-SWCNTs (Tables 2 and 3, Appendix A.).

It is known that the excitonic optical transition energies of SWCNTs are influenced by the environmental effect such as coating materials and solvents providing different local dielectric properties surrounding nanotubes [71,112,113]. Changes in the environmental dielectric constant modulate the dielectric screening of excitons, leading to spectral changes of electronic transitions including solvatochromic shifts (i.e., spectral

shift), changes in spectral width, and emissive quantum yields. Particularly, we observed a broad range of increase in nanotube PL intensity from 1.3-fold for $TTA(TAT)_2ATT$-(–) (6,5) to 14.7-fold for $CTTC_2TTC$-(8,3) hybrid with surfactant exchange. For example, fluorescence spectra of (9,4) species show that the E_{11} emission of SDC-coated (9,4) is significantly brighter with 12.8-fold increase in intensity, has a 6 nm decrease for the full width at half maximum (FWHM), and is blue-shifted by ≈ 7 nm, corresponding to the energy difference of 6.4 meV, compared with that of DNA-coated (9,4) (Figure 3.1.c.). These spectral changes demonstrate the sensitivity of nanotube PL to its surrounding environment where the complete displacement of DNA coatings by SDC leads to changes in the local dielectric constant. The observed fluorescence enhancement after DNA/SDC exchange could be due to the improved, uniform surface coverage by SDC, shielding nanotubes from the surrounding solution [113]. In addition, the pH of purified DNA-SWCNT samples prepared in water remained relatively stable during the short time period of surfactant exchange experiments. Consequently, we utilized fluorescence spectra to analyze kinetics of DNA displacement for all (*n, m*) SWCNT samples in water.

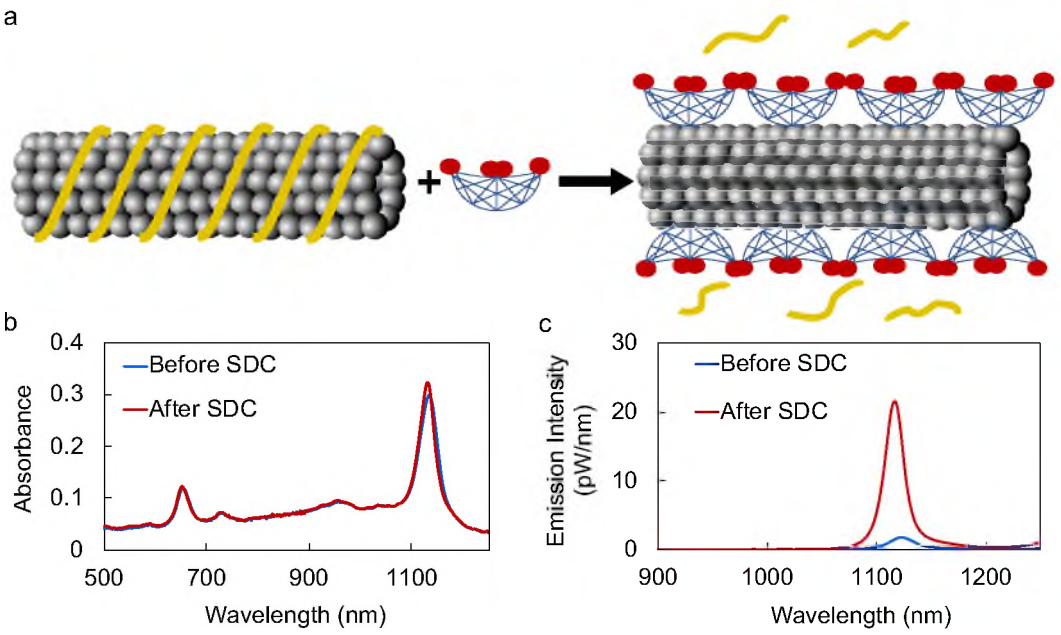

Figure 3.1. Schematic of DNA/SDC exchange process and corresponding optical characterization of purified CTTC3TTC-(9,4) species. (a) Displacement of DNA surface coating on a nanotube by SDC. (b) Absorbance and (c) fluorescence spectra for purified (9,4) species before and after adding SDC at equilibrium.

3.3.2. Kinetics of DNA displacement of pure-chirality SWCNTs by a surfactant

Because pure-chirality SWCNTs were employed, the evolving fluorescence spectra with time allowed us to extract defined spectral characteristics of the E_{11} emission peaks of (*n, m*) nanotubes to build simple kinetic models of DNA coating displacement. An example is shown for $T_4C_4T_4$-(11,1) enriched species in Figure 3.2. Clearly identifiable spectral modulations in emission intensity, line width, and peak position can be observed as DNA coatings being displaced by SDC. Interestingly, although (9,4) and (11,1) species have the same tube diameter, they showed distinct optical properties due to different surface coverage of molecules. Specifically, the E_{11} emission intensity of (11,1) species gradually increased up to 10.9-fold accompanied by a significant narrowing of spectral line width with a decrease of ≈ 29 nm for FWHM and a blue shift of 14 nm (i.e.,

the energy difference of $\Delta E_{11} \approx 11.2$ meV) upon displacing DNA from nanotubes (Tables 2 and 3, Appendix A.). The large decrease in spectral line width observed for this hybrid may be due to the contamination of (10,3) species, resulting in a broader E_{11} peak for the initial $T_4C_4T_4$-(11,1) sample (Figure 1, Appendix A). Regardless, we observed these combined optical phenomena of the brightening of nanotube PL, the narrowing of line width, and the blue shift in E_{11} peak wavelength for the majority of SWCNT samples as the surface structures transition from DNA-wrapped coatings, DNA conformational change and displacement by SDC to an improved surface coverage by SDC coatings. An exception is observed for the $CTTC_2TTC$-(8,3) hybrid, which did not show an apparent wavelength shift despite the 14.7-fold increase in E_{11} emission intensity and a narrower spectral shape for SDC-coated SWCNT (SDC-SWCNT). Because consistent increase in emission intensity was obtained for each (*n, m*) species with clearly identifiable optical transition peaks within the experimental time period, we analyzed kinetics of DNA coating displacement by investigating the change in emission intensity at the E_{11} peak wavelength of SDC-SWCNTs as a function of time.

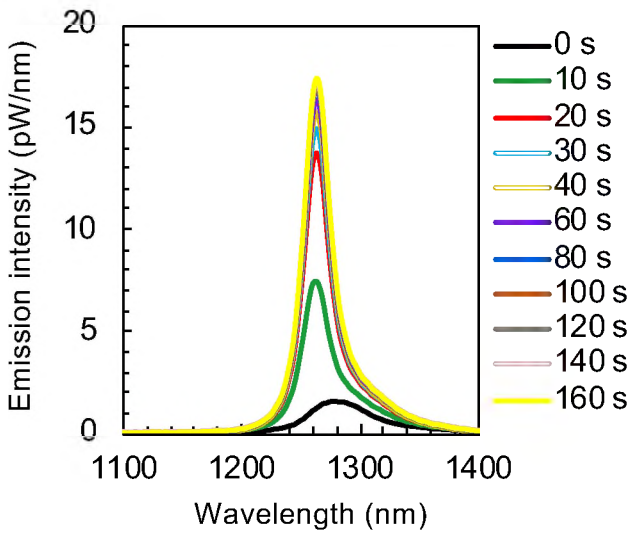

Figure 3.2. Time-resolved fluorescence spectra for purified $T_4C_4T_4$-(11,1) species showing distinct spectral changes in the E11 emission peak during DNA displacement by SDC. Samples were excited at 641 nm.

Each purified (*n, m*) SWCNT exhibits clear E_{11} emission peak during DNA displacement by surfactant. Figure 3.3. plots the time dependence of emission intensity ratio I/I_O of nanotubes at the E_{11} peak wavelengths of (*n, m*) SWCNTs, where I and I_O are the magnitude of emission peaks corresponding to SDC- and DNA-coated (*n, m*) SWCNTs. The time traces of increase in intensity ratio for all SWCNT samples can be modeled using single exponential fit (Table 4, Appendix A., $R^2 > 0.9$ for all fits from three repeats). This suggests that our surfactant exchange reaction operates as a pseudo-first order reaction as proposed for prior studies on ssDNA displacement kinetics using SWCNT mixtures [31,107,108]:

$$\text{DNA-}(n, m)\ \text{SWCNT} + \text{SDC} \xrightarrow{k} \text{SDC-}(n, m)\ \text{SWCNT} + \text{DNA}$$

where k is the rate constant corresponding to the inverse time constant $1/t$ obtained from the exponential fit.

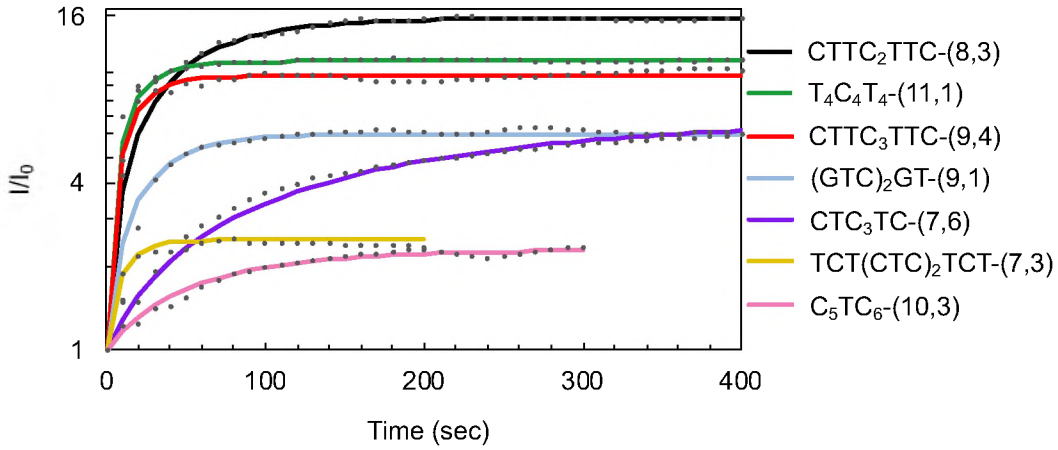

Figure 3.3. Measured (dotted lines) and exponential fits (solid curves) of fluorescence kinetics for purified DNA-(*n, m*) SWCNT samples during SDC exchange showing distinct responses in intensity ratio change for each (*n, m*) species at the E_{11} peak wavelength of nanotubes coated by SDC.

3.3.3. Comparison of distinct DNA displacement kinetics for (6,5) enantiomers

Additionally, we tested a pair of (6,5) enantiomers that are coated with the same recognition sequence $TTA(TAT)_2ATT$ to demonstrate the importance of (*n, m*) chiral structure on the interaction of nanotubes with DNA. Because of the difference in coating structure of the same DNA on the two enantiomers, kinetics of surfactant exchange showed different behaviors for the two (6,5) samples (Figure 3.4.). Specifically, (+) (6,5) showed a smaller blue shift of nearly 5 nm, a slightly larger increase in emission intensity (1.6-fold vs. 1.3-fold), and a shorter time constant (≈ 19 s vs. ≈ 52 s) compared with that of (–) (6,5) sample. These indicate that the hybridization affinity of the recognition DNA sequence is stronger for the (–) (6,5) than its mirror image (+) (6,5). The observed difference in DNA displacement kinetics by a surfactant for (6,5) enantiomers suggests that different enantiomeric forms of the same (*n, m*) species may induce drastic

differences in interactions between SWCNTs and various molecules of interest. This has potential implication in developing optical probes for detecting chiral molecules.

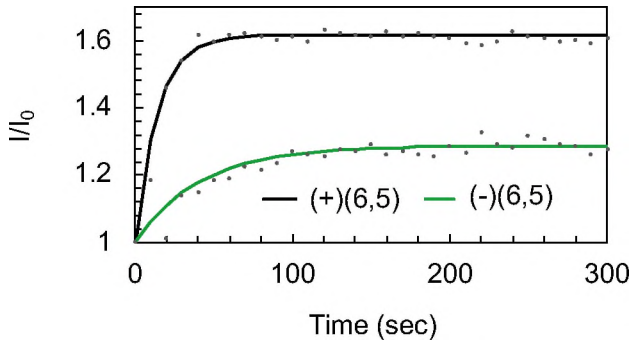

Figure 3.4. Fluorescence kinetics for purified (±) (6,5) enantiomers during displacement of the same TTA(TAT)2ATT coating by SDC showing different responses in intensity ratios at the E11 peak position of SDC-(±) (6,5). Dotted lines are experimental points and solid curves indicate the exponential fits for each enantiomer.

3.3.4. Analysis of spectral changes in E_{11} emission peaks of nanotubes with surfactant exchange

The distinct SWCNT chirality determines the diameter, chiral angle, and electronic structure of each (*n*, *m*) species. We plotted average spectral changes in E_{11} emission peaks of DNA-SWCNT recognition pairs after adding SDC as a function of nanotube diameter (d) and chiral angle (θ), respectively, indicating mod (*n*-*m*, 3) = 1 and mod (*n*-*m*, 3) = 2 semiconducting nanotubes [68] (Figure 3.5. and Figure 3 in Appendix A). Table 3 (Appendix A.) summarizes values corresponding to spectral changes that are obtained from three repeats. Metallic tubes that do not emit PL and have mod (*n*-*m*, 3) = 0 are not considered for this study. A broad range of PL intensity increase (i.e., I/I_O) from 1.3 to 14.7-fold was obtained for purified DNA-SWCNT hybrids tested, however no obvious correlations with either nanotube diameter or chiral angle were observed. Similarly, we did not observe obvious pattern for changes in spectral wavelength shift

($\Delta\lambda_{11}$), energy shift (ΔE_{11}), and line width (ΔFWHM) as a function of diameter and chiral angle, respectively, for each (*n, m*) species tested. This suggests that either diameter or chiral angle of nanotubes alone cannot account for spectral changes when displacing DNA coatings by surfactant. In addition, we considered the chirality effect of nanotubes on PL intensity ratios of DNA-SWCNT hybrids after surfactant exchange, but no obvious pattern was observed (Figure 4, Appendix A.). The absence of clear dependence of spectral changes on nanotube chirality for DNA/SDC exchange suggests the unique complexation of recognition DNA sequence and specific SWCNT species.

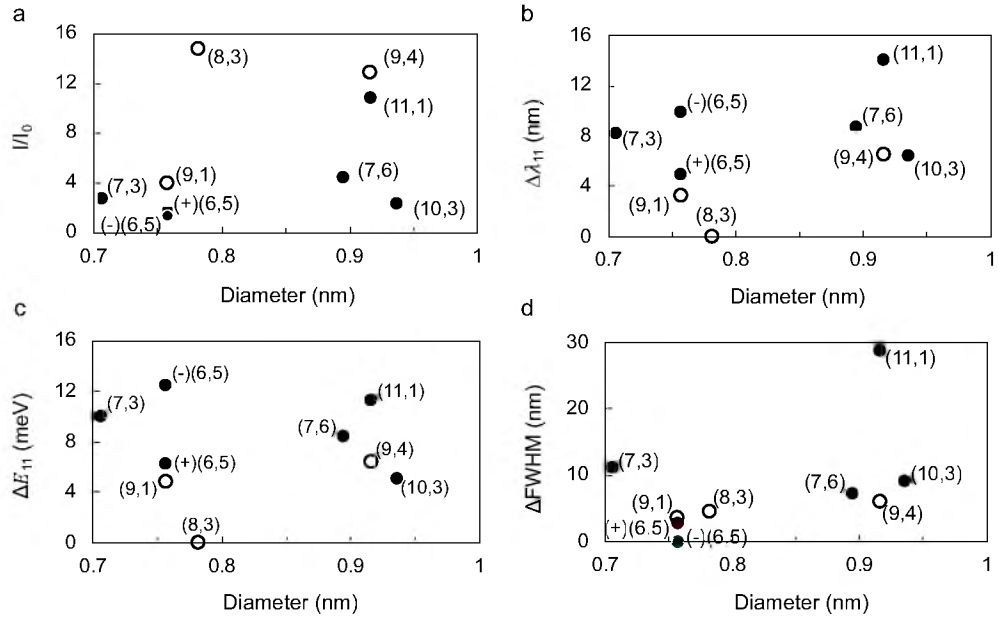

Figure 3.5. Spectral changes of E_{11} emission peaks of purified (*n, m*) SWCNT species as a function of nanotube diameter after DNA/SDC exchange at equilibrium. (a) PL intensity ratio increase, (b) wavelength and (c) energy shift, and (d) narrowing spectral line width of (*n, m*) species. Closed and open circles indicate mod 1 and mod 2, respectively.

We compared the interaction behavior of DNA sequences and SWCNTs based on the time constant obtained from spectral fit, where a longer time corresponds to a

stronger binding affinity of the recognition DNA sequence to a (*n, m*) species (Figure 3.5) [108]. We observed significant differences in deduced time constants among DNA-SWCNT recognition pairs with roughly 25-fold increase from ≈ 9 s for $TCT(CTC)_2TCT$-(7,3) up to ≈ 230 s for CTC_3TC-(7,6) hybrid (Table 4, Appendix A.). Among the (*n, m*) SWCNT species tested, (6,5) and (9,1) tubes have the same diameter of 0.757 nm, while the diameter of (9,4) and (11,1) tubes is 0.916 nm [68]. Although similar values were obtained for (9,4) and (11,1) tubes, the deduced time constants of purified DNA-SWCNT hybrids showed no clear correlation to the nanotube diameter (Figure 5, Appendix A.). Previously, larger time constants were observed for longer DNA length when dispersing SWCNT mixture samples using 6-mer to 60-mer ssDNA sequences [108]. However, DNA length is found to be not a factor affecting the time constants in our work as we utilized short recognition sequences of 7-mer to 12-mer. In fact, the stable CTC_3TC-(7,6) hybrid is complexed with the shortest DNA length (7-mer) tested, demonstrating the potential of short sequences for achieving improved nanotube sorting and stability of DNA-SWCNT hybrids in aqueous environments.

Pure-chirality DNA-SWCNT hybrids used in this work were separated in polymer ATP systems where the partition of the hybrid between the two phases is driven by the small difference in the surface functionality (i.e., the solvation free energy of the hybrid) [66,101]. It was proposed that the solvation free energy of a DNA-SWCNT hybrid is sensitive to the exact spatial distribution of hydrophilic groups (i.e., sugar-phosphate backbone of DNA that is exposed to water) along the nanotube axis, which is directly related to the wrapping pattern of DNA on the nanotube surface. Molecular dynamics simulations [34,38] of recognition pairs of DNA and SWCNT showed an ordered

wrapping structure of the DNA sequence on the SWCNT chirality, which leads to the differentiation of its solvation energy by the ATP system from all other DNA/SWCNT combinations. Our data provide quantitative comparisons of the complexation of recognition DNA sequence and specific SWCNT species, however, the elucidation of underlying structural differences in the ordered structure of each DNA-SWCNT hybrid will benefit from computational work in future studies. Regardless, the relatively low PL intensity increase, and longer time constants obtained for CTC_3TC-(7,6) with surfactant exchange suggest improved surface coverage of DNA coatings on the nanotube as well as a stronger hybridization affinity of the hybrid. Additionally, this CTC_3TC-(7,6) hybrid highlights the potential of short DNA sequences for separating and stabilizing pure-chirality nanotubes in aqueous environments.

3.3.5. Optical characterization of purified DNA-SWCNTs in cell culture media

Recent studies utilizing the purified $CTTC_3TTC$-(9,4) hybrid showed that pure-chirality SWCNTs exhibit long-term biocompatibility [4,20]. In addition to surfactant solutions, we characterized optical properties of purified DNA-SWCNT hybrids in cell culture media with and without serum. We identified $CTTC_3TTC$-(9,4) as one of the two hybrids, another hybrid being $(GT)_{20}$-(8,4), that showed negligible changes in fluorescence intensity during 8 hour incubation in 10 % FBS-containing cell culture media (Figure 3.6.). The stable hybrid CTC_3TC-(7,6) identified from our previous analysis of DNA coating displacement exhibited increase in fluorescence intensity, while varying levels of decrease in intensity were observed for the remaining hybrids (Figure 3.6.). In addition, we observed negligible changes for absorbance and emission spectra of purified DNA-SWCNT hybrids after incubation in cell culture media with serum, an

example of which is shown for the (–) (6,5) species at both room temperature and 37 °C (Figure 6, Appendix A.). Specifically, a red shift (i.e., increase in wavelength) in E_{11} emission peak was absent for several purified DNA-SWCNT hybrids and minimal red shifts of 1-3 nm (i.e., $\Delta E_{11} < 3.2$ meV) was observed for (7,3), (8,3), (7,6), (9,4), and (10,3) tubes. In comparison, DNA-SWCNT samples prepared from a synthetic nanotube mixture generally showed a spectral red shift (e.g., ΔE_{11} up to 7.7 meV with 6 hour incubation) [104] in serum-containing cell culture media due to electrostatic interactions of serum proteins and the phosphate backbone of DNA, which can cause nanotube aggregation [114]. Overall, negligible changes in absorbance spectra of purified DNA-SWCNT hybrids were observed for incubation in cell culture media with serum (Figure 7, Appendix A.), suggesting minimal nanotube aggregation.

However, several purified DNA-SWCNTs exposed to cell culture media without serum showed decrease in the E_{11} absorbance values indicating the formation of nanotube aggregations and diminished nanotube stability (Figure 8, Appendix A.). It is possible that the presence of serum proteins in cell culture media facilitates the dispersion stability of ordered DNA-SWCNT hybrids through forming a protective surface coating and preventing nanotube aggregation in cell culture media. In addition, the difference in pH of cell culture media with and without serum (i.e., pH 7.54 and 8.30, respectively) could possibly contribute to the different behaviors of purified DNA-SWCNT samples. Future studies on the effects of proteins and pH of cell culture media on the dispersion stability of purified DNA-SWCNTs will provide insights on the observed discrepancy in spectral stability of nanotubes in cell culture media with and without serum.

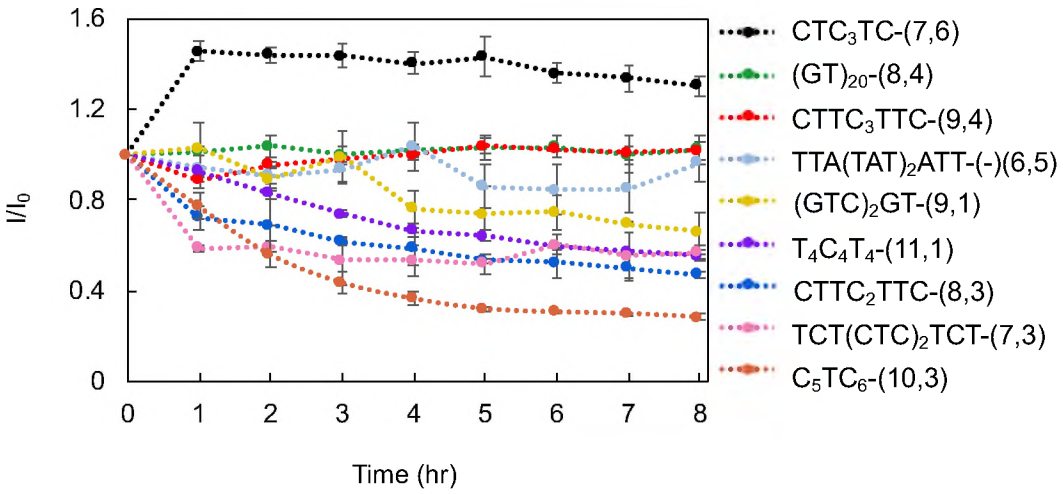

Figure 3.6. Intensity ratio at E_{11} emission peak position of purified DNA-SWCNTs as a function of time in 10 % FBS-containing cell culture media at room temperature.

3.4. Conclusions

In summary, we have demonstrated the distinct complexation of pure-chirality SWCNTs and recognition DNA sequences in various aqueous environments, providing valuable insights for optical and physicochemical properties of many purified DNA-SWCNT hybrids that have not been achieved previously. Particularly, purified DNA-SWCNT hybrids showed a broad range of increase from 1.3-fold to 14.7-fold in nanotube PL intensity in the NIR with surfactant exchange. Moreover, the time constants obtained from fitting intensity increase in NIR fluorescence of purified DNA-SWCNT hybrids showed more than an order of magnitude difference ranging from 9 to 230 s, clearly showing distinct complexation of each DNA-SWCNT recognition pair. In addition, purified DNA-SWCNTs incubated in cell culture media with serum showed improved spectral stability compared to that of serum-free cell culture media. In this work, the potential of short DNA sequences in manipulating nanotubes was highlighted by a special hybrid CTC_3TC-(7,6), which could have potential application as a stable optical probe for detecting targeted molecular interactions in biology. It also provides new possibilities of

creating unique DNA-SWCNT hybrids through the complexation of a pure-chirality SWCNT species, for example (7,6) tubes, with a DNA sequence of choice by combining the DNA/surfactant exchange and its reverse reaction, aided by methanol [115,116]. Our work provides a foundation for future studies involving carbon nanotube sorting and surface functionalization of pure-chirality SWCNTs to create multicolor, fluorescent molecular probes for applications such as bioimaging and biosensing.

CHAPTER IV

COVALENT FUNCTIONALZATION

4.1. Introduction

Surface modification of carbon nanotubes has gained interest due to the vast possibilities for tunability of the electronic structure and property enhancement, and for the applications that it enables, including imaging[29,30] and sensing, optoelectronic devices,[22] and photonics.[22–24] Specifically, covalent modification of single-wall carbon nanotubes (SWCNTs) is of growing interest at the present time. It has been achieved using bleach,[30] ozone,[117–119] diazonium salts,[25–27] and organic groups.[28] It has been shown that covalent functionalization can yield brighter PL and longer exciton lifetimes,[120] making SWCNTs more detectable for imaging,[30,117] in addition to providing a source for single photon emission[24,121] and other optoelectronic applications. Covalent functionalization can be achieved in two ways: through covalent oxygen doping[117] where all carbon atoms are still sp^2-hybridized, and through creation of sp^3 defects on the sp^2 carbon lattice of SWCNTs.[25,26] Surface modification due to either doping or chemical defects, enables the trapping of luminescent surface excitons at the functionalization sites allowing them to emit light more brightly than the original PL.[23,121]

In addition to doping molecules or functional groups, surface coating, solvent environment, and light source can have an effect on the efficiency of covalent reactions. Different solvents have been utilized including deuterium oxide (D_2O) and surfactant solutions in D_2O[25,26] as well as organic solvents.[27] The solvent plays an important role during the reaction and also affects the lifetime of the defect-generated PL.[122] Furthermore, surface coating of SWCNTs plays a significant role during the covalent modification reactions. Depending on the surfactant identity, the doping effect can either be facilitated or inhibited.[30] In this section, we explored covalent functionalization of SWCNTs through oxygen doping and the attachment of glycopolymers with a chain-end light-activatable phenyl azide moiety.

4.1.2. *Oxygen doping*

Ghosh et al. were the first to observe the oxygen doping effect on SWCNTs when treated with ozone.[117] Since then, researchers have used ozone treatments on SWCNTs and observed that oxygen doping is dependent on surface coverage of SWCNTs. For instance, when treating air-suspended SWCNTs with ozone, followed by UV light exposure, the oxygen doping effect seems to occur within 20 seconds,[118] as opposed to aqueous suspended surfactant-coated SWCNTs which can take up to 16 hours.[117] Here, we used a simple method for oxygen doping of pure-chirality (6,5) and other chirality SWCNTs including (6,5) enantiomer, (7,3), (7,6), (8,3), (9,1), (9,4), (10,3), and (11,1), in deionized (DI) water by shining short wavelength UV light, without additional treatments. Our work demonstrates that the efficiency of the oxygen doping reaction on (6,5) SWCNTs is a surface event and may be chirality or diameter dependent.

Additionally, we explored covalent functionalization of (6,5) SWCNT with disaccharide lactose containing glycopolymers with a chain-end phenyl azide group.

4.2. Experimental Section

4.2.1. Glycopolymer synthesis

All solvents and reagents were purchased from Sigma-Aldrich (USA) and were used as received. Deionized (DI) water with a resistivity of 18 MΩ cm was used as solvent in all reactions and dialysis experiments. Biomimetic glycopolymers with monosaccharide and disaccharide groups were synthesized via cyanoxyl free radical-mediated polymerization (CFRMP) scheme in one-pot fashion as previously reported.[123,124] In essence, cyanoxyl radicals were generated by an electron-transfer reaction between cyanate anions from a sodium cyanate aqueous solution and aryl-diazonium salts, which were prepared in situ through a diazotization reaction of arylamine in water. Cyanoxyl persistent radicals and aryl-type active radicals were simultaneously produced, where only the latter species was capable of initiating chain growth, thus facilitating the copolymerization of *N*-acryloyl-glycosylamine glycomonomers (Glyco-AM) and free acrylamide (AM).[123,124] Particularly, glycocopolymers (i.e., AM/Glyco-AM) expressing different densities of carbohydrate ligands (i.e., *y*/*x*) were synthesized by varying the ratios between *N*-acryloyl-glycosylamine glycomonomers and free acrylamide. Lact-homopolymers of various chain lengths *n* was synthesized by varying the amount of *N*-lactosylacrylamide monomer without inclusion of free acrylamide.

4.2.2. Photochemistry: oxygen doping and glycopolymer immobilization

Samples were diluted in DI water for an absorbance of 0.1 OD (0.08 to 0.12) at E_{11}, which corresponds to approximately 0.65 ug/mL concentration of SWCNT,[111] for

a total volume of 150 uL for oxygen doping or 200 uL glycopolymer photochemistry. Samples were exposed to 254 nm and 356 nm UV light of 8W at a power density of ~13 mW/cm^2 for the desired time. For oxygen doping, samples were left exposed to environmental air for 30 minutes before UV light exposure. A similar procedure was followed for photochemistry with glycopolymers. SWCNTs were diluted in D_2O and absorbance was adjusted to around 0.1 OD at E_{11}. Then, the desired volume of glycpolymer to be added was calculated based on the desired SWCNT : glycopolymer mass ratio. Glycopolymer powders were stored at -20°C. Glycopolymer stock solutions were prepared in either 2mg/mL or 1 mg/mL concentrations in order to only add a small aliquot and not disturb the SWCNT sample. Glycopolymer solutions were used immediately as prepared. Glycopolymer stock solutions were protected from environmental light and kept at 4°C. SWCNT samples, after adding the glycpolymer, were also protected from environmental light. Samples were bath sonicated for 15 minutes at room temperature after addition of glycopolymer. Samples were then put into quartz cuvettes and tightly sealed with a rubber stopper, to facilitate the oxygen removal procedure.

Oxygen removal was performed through a needle connected to a vacuum pump (8907, Welch). Samples were left under vacuum for a few seconds up to a minute until bubbles were no longer formed. Then, the vacuum needle was switched for the needle connected to an Argon (Ar) gas tank in order to purge the sample with Ar and replace air in the cuvette. This process took only 1-2 seconds due to the low volume of the cuvette. The process of vacuum to purging with Ar was repeated for at least three times to ensure bubbles were no longer formed. Vis-NIR Absorbance, NIR fluorescence, and Raman

spectra were measured before and after the oxygen removal process. Lastly, samples were exposed to UV light for the desired time, over an ice bath to ensure samples did not heat. Spectra were measured after UV exposure.

4.3. Results and Discussion

4.3.1. Oxygen doping

As a quasi-one-dimensional nanomaterial, SWCNTs are of high interest for covalent modification, as all atoms are exposed to the surface. Covalent functionalization has been explored in the recent years particularly via oxygen doping. It has been shown that oxygen has an affinity for the nanotube surface, either via redox reactions[111] where oxygen molecules occupy atomic sites or via excited states of oxygen known as oxygen singlets ($^1O_2$) attaching to nanotube surfaces and causing permanent alterations to the nanotube structure. Figure 4.1. shows a schematic of the oxygen attachment to the nanotube surface.

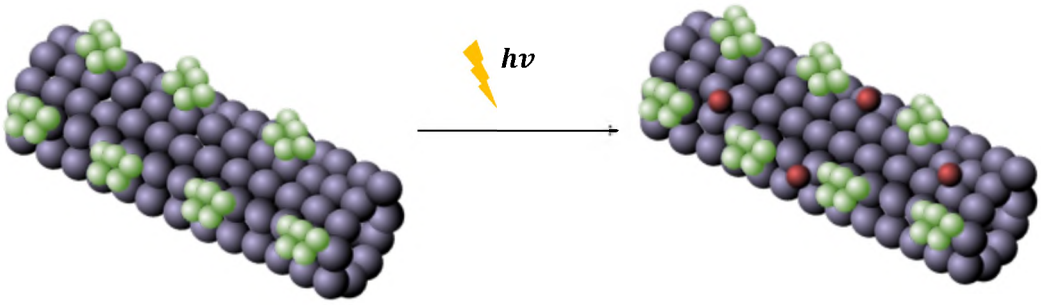

Figure 4.1. Schematic of oxygen doping of SWCNT-surfactant upon UV light exposure. Green spheres represent surface coating molecules. Red spheres represent oxygen singlet molecules.

We explored the oxygen doping effect on chirality-pure SWCNTs in DI water, exposed to long and short UV wavelengths (Figure 4.2.). We saw that oxygen doping was more efficient at shorter UV wavelengths, as can be seen from the E_{11}^- peak

formation under exposure to 254 nm. No evidence of a new E_{11}^- peak was seen for 365 nm UV wavelengths, which could be due to the energy difference between the 254nm and 365 nm UV light and its effect on the excitation of oxygen singlet molecules.[91] Raman spectroscopy was also measured (Figure 11, Appendix B.). However, no significant "D" peak can be seen, which may be due to the highly diluted sample at absorbance ~0.1 OD. Additionally, we tested oxygen doping for (6,5)-SDBS after removing dissolved oxygen in the solution and purging with Argon (Figure 16, Appendix B.). The E_{11}^- peak formation is much lower when the sample is purged with Ar, as compared to unpurged sample (Figure 4.2.a).

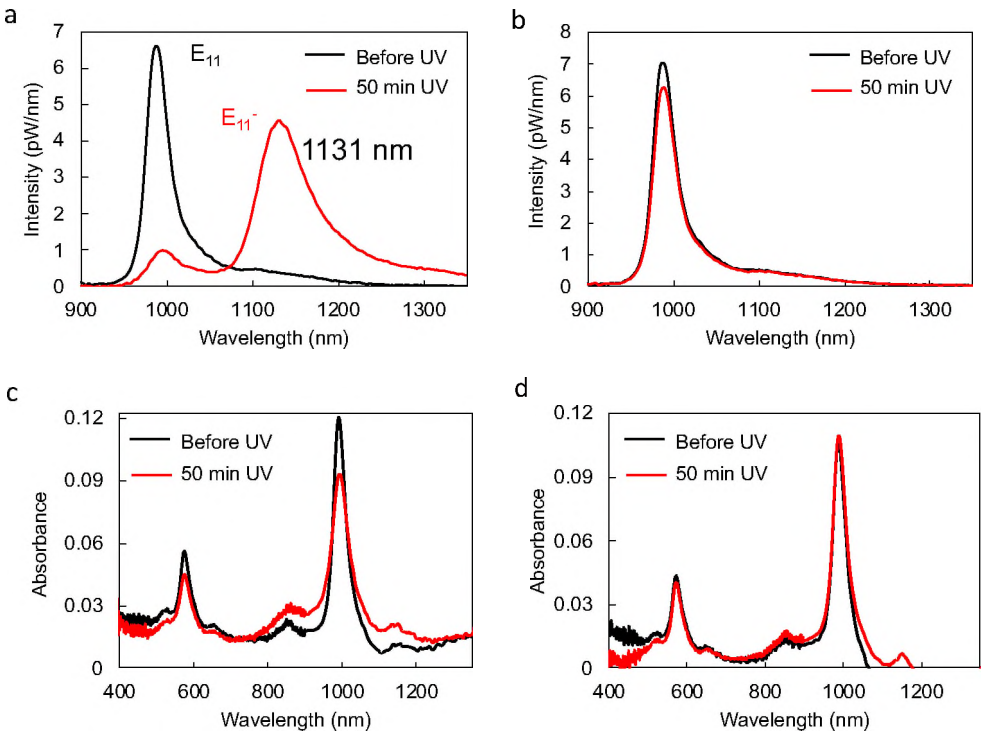

Figure 4.2. a) Oxygen doping gives rise to a new fluorescence peak, E_{11}^- for (–)(6,5)-SDBS. c) Absorbance before and after exposure to 254 nm UV light. b) Emission intensity and d) absorbance of (–)(6,5)-SDBS before and after exposure to 365 nm UV light.

To find the optimal reaction efficiency, we investigated the oxygen doping at different time intervals to find an optimal exposure time (Figure 4.3.a.). E_{11}^- peak formation due to oxygen doping started before 20 minutes and proved to be more efficient around 50 minutes of UV exposure, after which the E_{11}^- peak started to decrease. Additionally, we plotted the dimensionless emission intensity of the E_{11}^- and E_{11} peak at different times (Figure 4.3.b.). Figure 4.3.b. clearly shows the E_{11}^- peak intensity is the highest at 50 minutes and decreases gradually for longer exposure times until it reaches almost zero after 3 hours. The original E_{11} peak decreases by half at 20 minutes exposure time and reaches zero after 90 minutes of UV exposure due to the excitons being trapped at the created "defect" sites, decreasing mobility along the nanotube axis. Moreover, long exposure increases the quantity of excess defects along the SWCNT wall, leading to irreversible quenching of both E_{11} and E_{11}^-. In addition, we plotted the dimensionless E_{11} absorbance as a function of UV exposure time (Figure 9, Appendix B.). Absorbance is relatively stable, with minimal aggregation occurring up to 40 minutes of exposure and remains relatively constant for the duration of the 3-hour experiment.

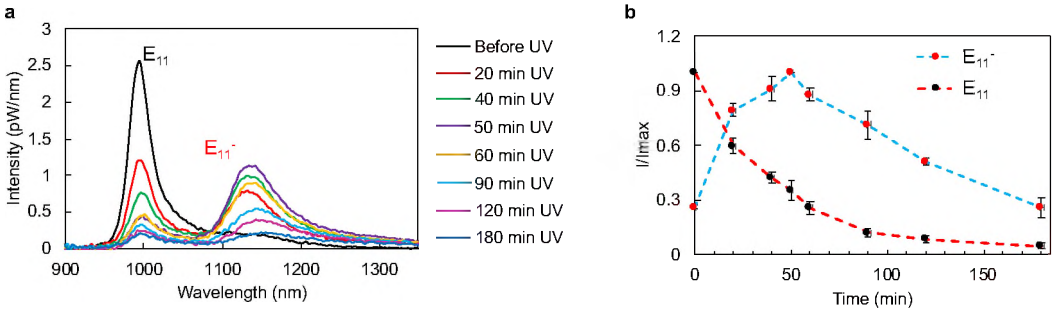

Figure 4.3. E_{11}^- created from oxygen doping, is sensitive to UV exposure time. a) Emission intensity of (–)(6,5)-SDBS at different exposure times to 254 nm UV light. Oxygen doping is most efficient at 50 min UV exposure. b) Dimensionless intensity of (–)(6,5)-SDBS at different UV exposure times; I is the emission intensity at different times and I_{max} is maximum emission intensity, for E_{11} and E_{11}^-. Dashed lines are there to guide the eye.

It has been shown that covalent modification of SWCNTs, including oxygen doping via bleach[30] or ozone,[29] is highly dependent on the coverage of the nanotube surface. Surfactant-coated SWCNTs have been successfully employed for covalent attachment experiment via diazonium reactions.[25,26] We performed oxygen doping experiment on the same chirality-pure SWCNT species, (–)(6,5), covered by different coating molecules including their recognition DNA sequence and surfactants (Figure 4.4.). It can be seen that DNA (Figure 4.4.a.) and SDC (Figure 4.4.b.) show no E_{11}^- peak formation even though there is a decrease in E_{11}. It is known that DNA forms ordered structures on the nanotube surface and SDC is a strong surfactant that covers most of the nanotube surface which could explain why oxygen doping is least efficient. However, the trend tends to be less clear when comparing other surfactants. SDBS (Figure 4.4.d.) is not the weakest surfactant but it proves to be the most efficient for oxygen doping, with an E_{11}^-/E_{11} intensity ratio of 0.66 and ΔE_{11} of 159 meV (Table 4.1.). The reaction efficiency is then followed by SDS (Figure 4.4.e.) and SC (Figure 4.4.c.), with ΔE_{11} of 160 and 123 meV (Table 4.1.), respectively. These results are different from oxygen doping results obtained by Lin et al. using bleach, where SDBS was the least efficient and SC was the most efficient.[30] Our results suggest that there may be a different mechanism behind the oxygen doping effect in our case, dependent on the coating material rather than the nanotube surface coverage. Additionally, oxygen doping for (6,5)-SDS and (6,5)-SC after removing dissolved oxygen in the solution and purging with Argon are shown in Figure 16, Appendix B, for reference. E_{11}^- peak formation is less efficient when oxygen is removed from the sample.

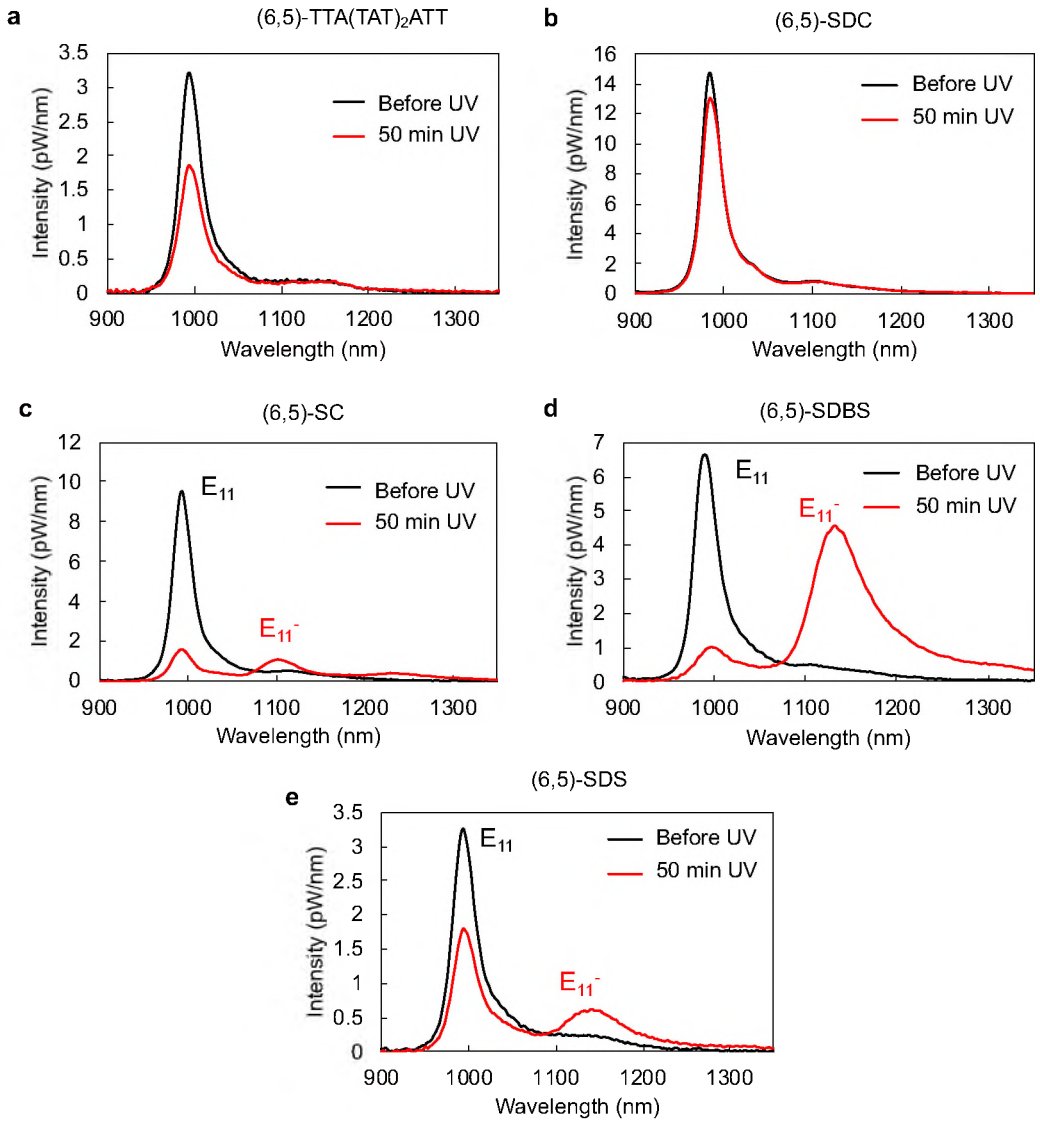

Figure 4.4. Emission intensity of (–)(6,5) SWCNT with different surface coating before and after exposure to 254 nm UV light. E_{11}^- formation varies in intensity and wavelength, and is most efficient for (–)(6,5)-SDBS (d).

Table 4.1. E_{11}^- intensity, wavelength, and energy shift show strong dependence on surface coatings of (–)(6,5) upon exposure to 254 nm UV for 50 minutes.

SWCNT	E_{11} (nm)	E_{11}^- (nm)	ΔE_{11} (meV)	E_{11}(pW/nm)	E_{11}^- (pW/nm)	E_{11}^-/E_{11}
$TTA(TAT)_2ATT$ -(–) (6,5)	995.1±0.0	-	-	3.35±0.10	-	-
SDC-(–)(6,5)	985.2±0.0	-	-	10.00±3.32	-	-
SC-(–)(6,5)	993.5±0.0	1101.8±0.0	122.7±0.0	10.20±0.72	0.99±0.06	0.09±0.01
SDBS-(–)(6,5)	988.0±0.7	1131.2±0.0	158.9±0.9	7.30±0.74	4.85±0.57	0.66±0.03
SDS-(–)(6,5)	995.1±0.0	1141.6±0.7	159.9±0.7	2.78±0.70	0.60±0.08	0.23±0.08

Various properties of SWCNTs, are known to be chirality dependent, which is also one of the reasons why it is important to utilize chirality-pure SWCNTs to understand their fundamental properties. To that end, we explored oxygen doping for various chirality-pure SWCNTs including the (6,5) enantiomers and same diameter SWCNTs. Figure 4.5. shows the oxygen doping effect for the mirror image of (–)(6,5), (+)(6,5) SWCNT. Similar results are shown for (+)(6,5), where DNA (Figure 4.5a.) does not allow oxygen doping, but SDBS (Figure 4.5b.) does. There is no significant difference for the two enantiomers in terms of E_{11}^- intensity or wavelength, or energy difference, ΔE_{11}, 158 vs 154 meV (Table 4.2.). (+)(6,5) has an E_{11}^- peak around 1123 nm, which correspond do the oxygen doping peak reported in previous literature, which is around 1120 nm,[117] whereas (–)(6,5) has an E_{11}^- peak around 1131 nm.

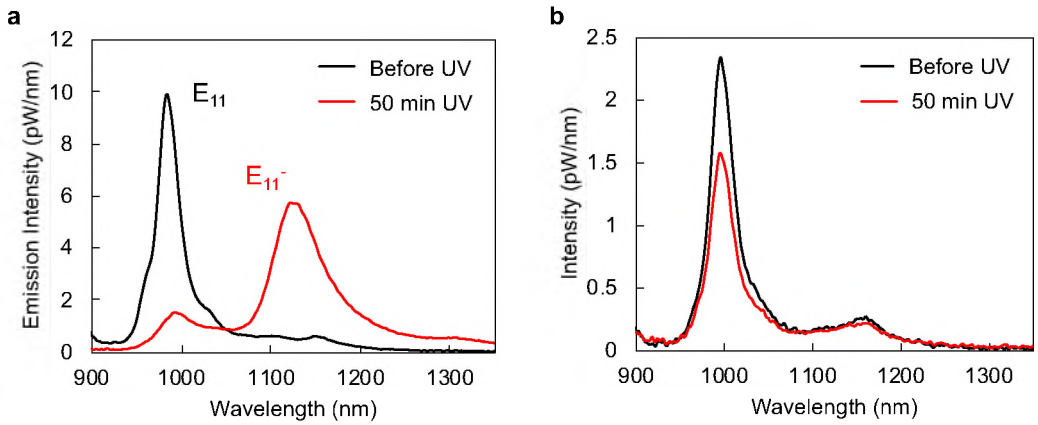

Figure 4.5. a) Formation of a new fluorescence peak, E_{11}^- for (+)(6,5)-SDBS, upon exposure to 254 nm UV light. b) Emission intensity for (+)(6,5)-DNA. Oxygen doping is surface coating dependent.

Additionally, we tested another chirality-pure SWCNT, (9,1), that has the same diameter as the (6,5) enantiomers (0.757 nm) (Figure 4.6.). Although the exposure time for (9,1) is only 20 minutes, due to sample aggregation at longer exposures, there was still an E_{11}^- peak formation. However, even though (9,1) has an E_{11} peak at lower wavelengths (922 nm) compared to (6,5), its E_{11}^- peak formed at 1140 nm, with a ΔE_{11} of 256 meV (Table 4.2.), 10 times as high as that of (–)(6,5) and (+)(6,5).

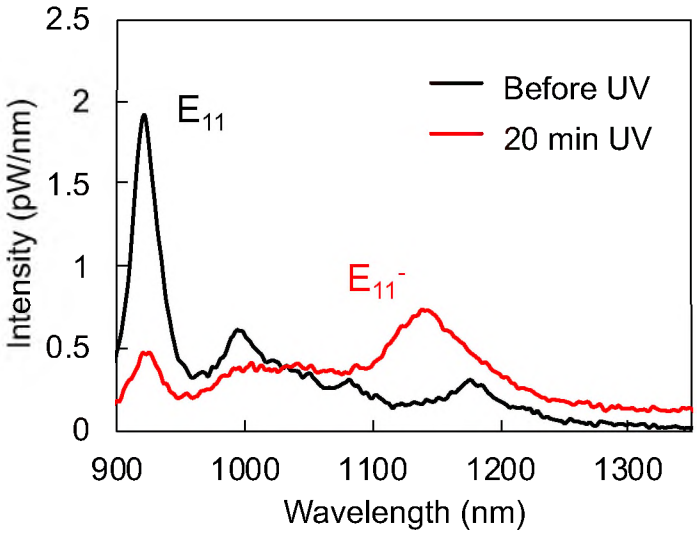

Figure 4.6. Formation of a new fluorescence peak, E_{11}^- for (9,1)-SDBS, upon exposure to 254 nm UV light for 20 min.

Moreover, we tested (7,3), (7,6), (8,3), (9,4), (10,3), and (11,1) SWCNT-SDBS species to further investigate chirality as well as diameter dependence of oxygen doping (Figure 4.7.). Exposure times are different because some nanotube species aggregated more at longer exposure times. Although the E_{11}^- peak intensity is not as high compared to (6,5) enantiomers, there seems to be a clear trend for different diameter tubes. For example, tubes with diameter larger than 0.8 nm show the smallest difference in ΔE_{11}, <110 meV (Table 4.2.), whereas for smaller diameter tubes the energy difference, ΔE_{11}, is greater than 150 meV. Additionally, (10,3), the largest diameter tube (0.936 nm) seems to have the lowest, almost non-existent, E_{11}^- peak. However, there is no clear trend for chirality dependence of oxygen doping. Same diameter tubes such as the (6,5) enantiomers and (9,1), as well as (9,4) and (11,1), show similar results in energy shifts. Overall, the E_{11}^- peak wavelengths ranged from 1123 nm for (+)(6,5) to 1378 nm for (10,3).

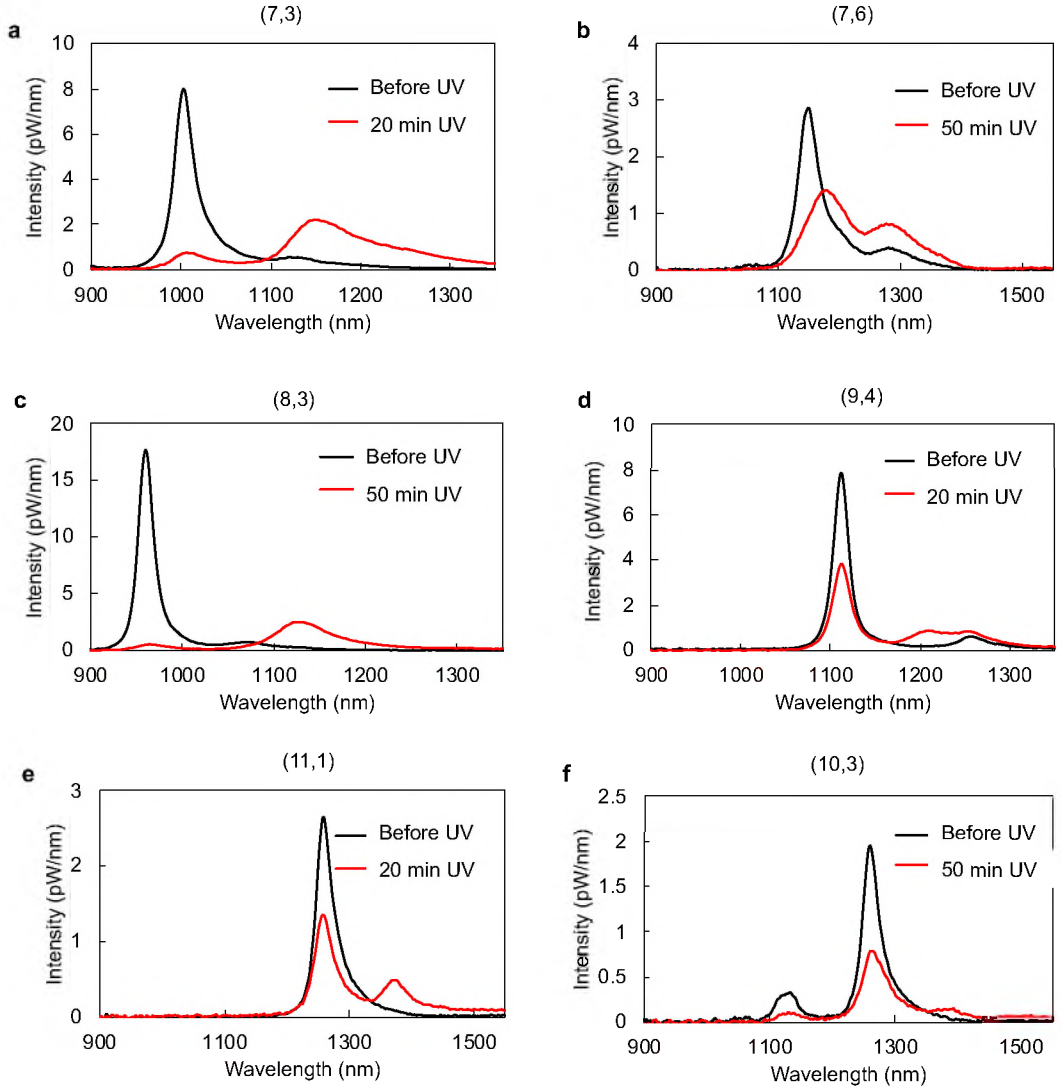

Figure 4.7. Oxygen doping for several chirality-pure SWCNTs coated with SDBS, at their optimal exposure times to 254 nm UV light. Oxygen doping may be diameter depended as larger diameter tubes show low intensity for E_{11}^{-}.

Table 4.2. List of chirality-pure SWCNTs and their spectral changes. E_{11}^- intensity, wavelength, and energy shift show dependence on nanotube diameter upon exposure to 254 nm UV for at their optimal exposure times.

SWCNT	d (nm)	E_{11} (nm)	E_{11}^- (nm)	ΔE_{11} (meV)	E_{11} (pW/nm)	E_{11}^- (pW/nm)	E_{11}^-/E_{11}	Time (min)
SDBS-(7,3)	0.706	1001.7±0.0	1149.7±0.7	159.4±0.7	8.75±1.81	2.24±0.19	0.27±0.07	20
SDBS-(–)(6,5)	0.757	988.0±0.7	1131.2±0.0	158.9±0.9	7.30±0.74	4.85±0.57	0.66±0.03	50
SDBS-(+)(6,5)	0.757	985.2±0.0	1123.0±0.0	154.5±0.0	9.79±0.21	5.90±0.19	0.60±0.02	50
SDBS-(9,1)	0.757	922.7±0.0	1140.5±0.7	256.8±0.7	1.87±0.05	0.68±0.06	0.36±0.02	20
SDBS-(8,3)	0.782	960.6±0.0	1125.2±3.0	189.0±3.0	17.74±0.00	2.75±0.17	0.15±0.01	50
SDBS-(7,6)	0.895	1148.1±0.7	1277.1±0.7	109.1±0.6	3.20±0.24	0.88±0.05	0.27±0.01	50
SDBS-(9,4)	0.916	1112.7±0.7	1210.0±0.7	89.7±1.4	8.51±0.99	1.51±0.85	0.16±0.07	20
SDBS-(11,1)	0.916	1257.1±0.7	1370.7±0.7	81.7±1.1	2.84±0.23	0.57±0.16	0.20±0.04	20
SDBS-(10,3)	0.936	1259.8±0.0	1378.7±0.7	84.9±0.4	2.16±0.19	0.16±0.02	0.07±0.00	50

4.3.2. Photochemistry with glycopolymers

We explored covalent attachment of SWCNTs with biomimetic glycopolymers with a chain-end functionalized aryl azide ($-N_3$) group. Theoretically, when exposed to UV light, $-N_3$ forms radicals, particularly the highly active nitrene,[87,88] that enable covalent attachment to C=C bonds in SWCNTs , and yield SWNCT-hosted organic color centers with oriented and immobilized glycopolymer (Figure 4.8.). A list of glycopolymers used and relevant information are provided in Table 5 and Figure 17, Appendix B.

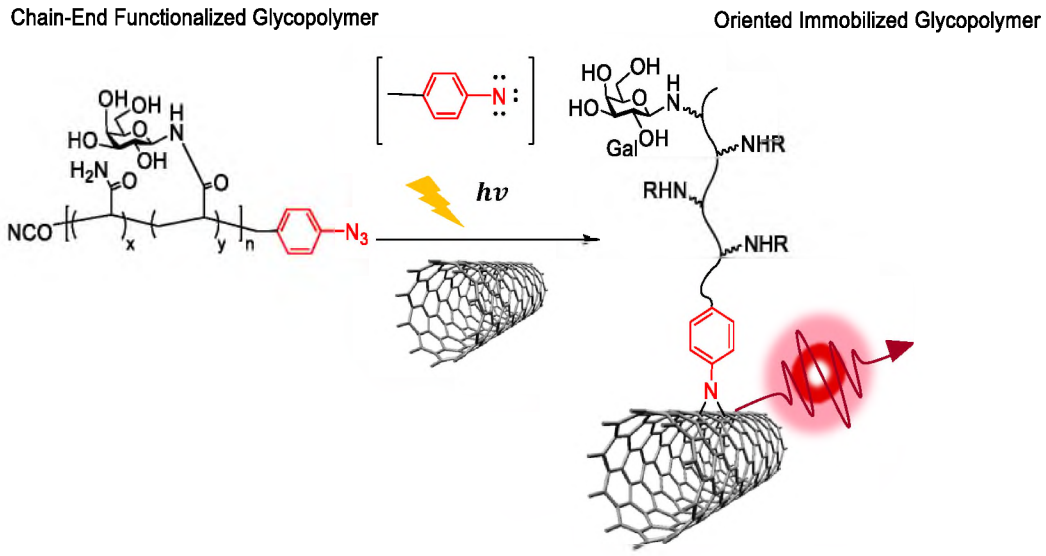

Figure 4.8. Schematic of covalent attachment of glycopolymers on the SWCNT surface upon exposure to UV light. (Courtesy of Dr. Xue-Long Sun)

The SWCNT used for this project is (–)(6,5) as it has been broadly employed for oxygen doping as well as covalent functionalization with aryl diazonium salts. We explored covalent functionalization of (6,5)-SDS with biomimetic glycopolymers in DI H_2O, with exposure to 254 nm UV light. For these experiment, dissolved oxygen was removed via vacuum and the samples were purged with Ar gas. The increase in fluorescence after purging with Ar, is due to the dissolved oxygen being displaced from the solvent, decreasing the oxidation effect that oxygen has on the SWCNT PL.[125] This is different from the permanent covalent attachment of oxygen on the SWCNT surface. Figure 4.9. shows the photochemical reaction of a Lactose-homopolymer (0:415), or Lac 415, with (6,5)-SDS exposed to 254 nm UV light for longer than one hour. There is a clear E_{11}^- peak formation around 1113 nm upon exposure to UV for 140 min for the 1:0.3 mass ratio of SWCNT : glycopolymer (Figure 4.9a.). Although, it not clear whether the new E_{11}^- peak is due to the $-N_3$ attachment or oxygen doping, as an E_{11}^- peak was also present for (–)(6,5)-SDS without addition of glycopolymer. However, this

peak is a lower wavelength than that of the oxygen doping for (–)(6,5)-SDS (Figure 4.4.e.). Additionally, there is an E_{11}^- peak formed for the 1:0.6 mass ratio of SWCNT : glycopolymer sample (Figure 4.9.b.). Similarly, this peak is at 1109 nm, whereas for oxygen doping with SDS, the E_{11}^- peak is around 1140 nm. Further characterizations are needed to confirm whether this new peak is due to the covalent attachment of phenyl azide group.

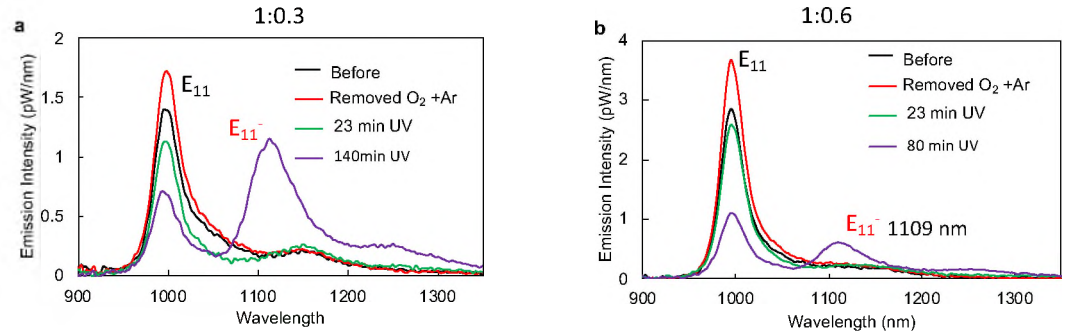

Figure 4.9. Photochemical reaction of (6,5)-SDS with Lactose-homopolymer (0:415) in H_2O, exposed to 254 nm UV light. The numbers in parenthesis represent the acrylamide backbone and chain length, respectively, of the glycopolymer. Mass ratios of SWCNT : glycopolymer are 1:0.3 in a), and 1:0.6 in b).

Because of the uncertainty of oxygen doping in the glycopolymer results, we decided to replicate the experiment in different solvents, including D_2O. It is known that the lifetime of oxygen singlets is shorter in D_2O than in H_2O. As such, we performed the photochemical reaction of (6,5)-SDS with Lac 415 in D_2O, exposed to 254 nm UV light for 1:0.6 mass ratio of SWCNT : glycopolymer (Figure 4.10.b.). There is a very slight formation of an E_{11}^- peak in Figure 4.10.b. that is not evident for (6,5)-SDS, which does not contain any glycopolymer (Figure 4.10.a.). This is one reason to further explore the photochemical reaction with Lac415 at longer UV exposures.

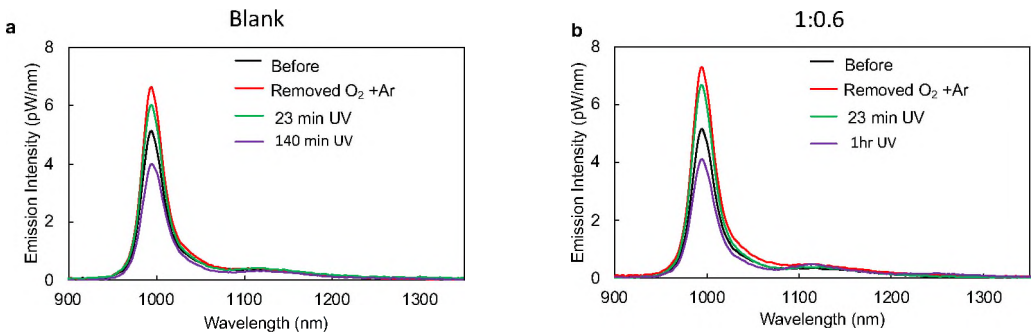

Figure 4.10. a) (6,5)-SDS in D_2O without addition of glycopolymer, exposed to 254 nm UV light. b) Photochemical reaction of (6,5)-SDS with Lactose-homopolymer (0:415) in D_2O, upon exposure to 254 nm UV light. The mass ratio of SWCNT : glycopolymer is 1:0.6. E_{11}^- formation is strongly dependent on solvent environment.

Additionally, we tested another solvent to explore its effect on the photochemical reaction. Figure 4.11. shows (6,5)-SDS with Lac 415 at a mass ratio of 1:0.6, in a 1 mass % SDS-D_2O solution, exposed to 254 nm UV light for 23 min. There is a significantly high E_{11}^- peak formed around 1095 nm, much lower than that reported for oxygen doping (1120 nm). The peak showed further increase after 20 hours of reaction in the dark. Because the E_{11}^- peak was also formed for a blank sample (no addition of glycopolymer) upon exposure to UV light (Figure 18.b., in Appendix B.), it suggests the need for further characterizations to confirm that it is from the covalent attachment of the phenyl azide group.

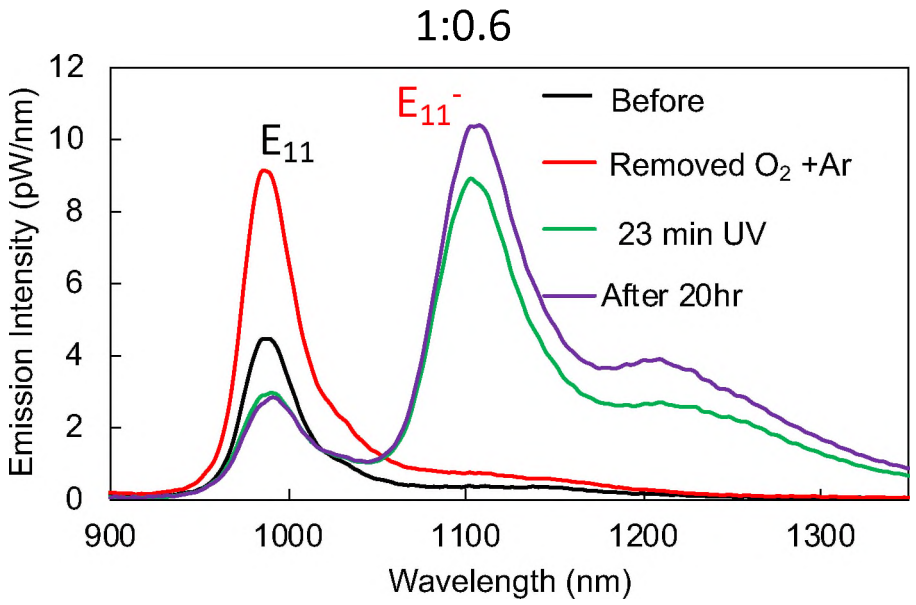

Figure 4.11. Photochemical reaction of (6,5)-SDS with Lactose-homopolymer (0:415) in 1% SDS-D_2O solution, upon exposure to 254 nm UV light. The mass ratio of SWCNT : glycopolymer is 1:0.6. E_{11}^- formation is strongly dependent on solvent environment.

In addition, we tested shorter length glycopolymer to see whether the photochemical reaction was dependent on polymer length, as previously reported covalent attachment reactions have been performed with shorter length molecules. Figure 4.12. a, b, and c, show the photochemical reaction of (6,5)-SDS with lactose-copolymer (4:1), or Lac 4:1, for different mass ratios of SWCNT : glycopolymer. There is a slight E_{11}^- peak formation for 1:6 mass ratio (Figure 4.12.) around 1116 nm. There seem to be two small E_{11}^- peaks formed after long exposure times (up to 180 min) for the glycopolymer containing sample (Figure 4.12.d.) as compared to the blank sample (Figure 18.a., Appendix B.). Longer exposure times as well as greater mass ratios of SWCNT : glycopolymer should be explored to see whether the E_{11}^- peak intensity will increase.

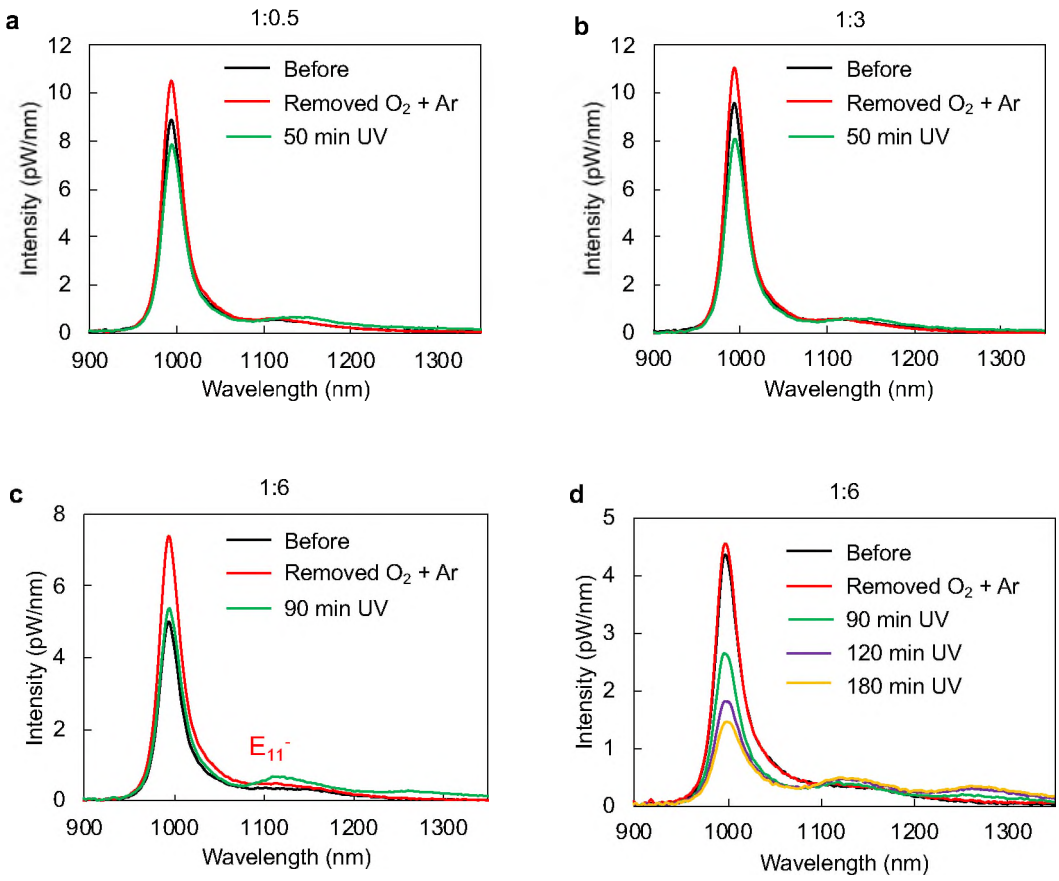

Figure 4.12. Photochemical reaction of (6,5)-SDS with Lactose-copolymer (4:1) in D_2O. Mass ratios of SWCNT : glycopolymer are given. A slight E_{11}^- peak is formed for 1:6 mass ratio of SWCNT : glycopolymer upon exposure to 254 nm UV light over 90 min (c and d).

Furthermore, we tested another short glycopolymer. Different mass ratios of Lactose-copolymer (1:1) were used for the photochemical reaction with (6,5)-SDS. The results of this reaction are shown in Figure 4.13. No E_{11}^- peaks were formed, even for longer exposure times. However, different ratios of glycopolymer should be tested in further experiments.

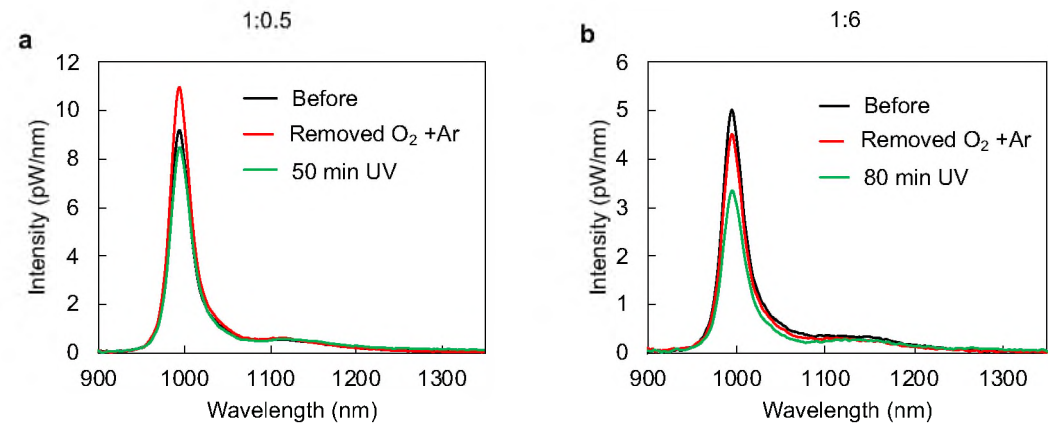

Figure 4.13. Photochemical reaction of (6,5)-SDS with Lactose-copolymer (1:1) in D_2O, upon exposure to 254 nm UV light. Mass ratios of SWCNT : glycopolymer are 1:0.5 in a), and 1:6 in b).

4.4. Conclusions

We show a simple and effective method for oxygen doping of different chirality SWCNTs, including (6,5) enantiomers, upon short wavelength UV light exposure. The efficiency of oxygen doping reaction was highly dependent on coating material on the nanotube surface and may be dependent on nanotube diameter. Consequently, SDBS-coated (6,5) showed the highest increase in a new E_{11}^- peak formation, and (10,3), the largest diameter nanotube was least efficient in E_{11}^- peak formation. Additionally, the amount of oxygen contained in the sample also affects the oxygen doping reaction.

Secondly, we showed preliminary data on covalent functionalization of SWCNTs with various glycopolymers. Lac 4:1 shows promising results for covalent attachment to the nanotube surface and should be focus of future work.

CHAPTER V

CONCLUSIONS

We have shown an extensive amount of work in elucidating the complexation of recognition DNA sequences with pure-chirality SWCNTs. Unique changes were observed for DNA-SWCNTs hybrids upon exchange with a strong surfactant, SDC, including distinct reaction time constants (9 s to 230 s) and an increase in PL (1.3 to 14.7-fold). Additionally, DNA-wrapped SWCNTs showed unique interaction behavior and stability in cell culture medium. The CTC_3TC-(7,6) hybrid exhibited the largest time constant upon surfactant-exchange and was the only hybrid to show an increase in near-infrared (NIR) fluorescence intensity in serum-containing cell culture medium. This hybrid could have potential in designing stable optical probes for detection of targeted molecular interactions in biology and should be a focus of future studies. Overall, these results offer insights for the optical and physiochemical properties of chirality-pure SWCNTs and provide a foundation for future development of applications for chirality-pure SWCNTs in biochemical sensing and imaging advancement.

Secondly, we show a simple method for oxygen doping of different chirality SWCNTs, including (6,5) enantiomers, upon short wavelength UV light exposure. The

efficiency of oxygen doping reaction was highly dependent on coating material on the nanotube surface and may be dependent on nanotube diameter. Consequently, SDBS-coated (6,5) showed the highest increase in a new E_{11}^- peak formation, and (10,3), the largest diameter nanotube was least efficient in E_{11}^- peak formation. Additionally, the amount of oxygen contained in the sample also affects the oxygen doping reaction.

Lastly, we showed preliminary data on covalent functionalization of SWCNTs with various glycopolymers. Lact 4:1 shows promising results for covalent attachment to the nanotube surface and should be focus of future work. Successful completion of this work could lead to a multifunctional hybrid with enhanced optical properties and potential to be utilized for protein sensing. Particularly, the sugar group can be selective towards a carbohydrate-binding protein, and carbohydrate-protein recognitions are important in many cellular functions.

CHAPTER VI

RECOMMENDATIONS AND FUTURE PERSPECTIVE

6.1. Surfactant Exchange and Stability in Biological Media

- Further experiments should be investigated for CTC_3TC-(7,6) hybrid in biological samples, to develop optical probes for detection of targeted molecular interactions.
- SDC is a chiral molecule, therefore, achiral surfactants should also be tested to see if the DNA-surfactant exchange could be chirality dependent, particularly, for the (6,5) enantiomers.
- Consequently, (6,5) enantiomers should be further investigated as they have potential in developing applications for detection of chiral molecules.

6.2. Oxygen Doping

- Oxygen doping for (6,5) enantiomers should be further explored, to be able to develop applications. For instance, the oxygen doped SWCNT can be tested in different solvent environment to see characterize the properties of the new E_{11}^- peak and its stability.
- More efforts should be made to better understand the mechanism behind oxygen doping, focusing on the UV light effect on the different coating materials.

6.3. Glycopolymer Photochemistry

- Oxygen doping can be a problem for successful photochemical reaction with glycopolymers, especially since oxygen doping and azide activation occurs around the same UV light wavelength (254 nm). Therefore, a more effective method of removing oxygen from solvent should be found.
- Different UV lights can be used, closer to those of phenyl azide photoactivation (265 to 275 nm).
- Test different mass ratios of SWCNT:glycopolymer, particularly for lact 4:1, to find optimal ratio.
- Test different UV exposure times, > 3 hours.
- Test different polymers.
- Try different direct and indirect characterization methods for the new E_{11}^- peak: FTIR, carbohydrate sensing proteins.

REFERENCES

[1] Y. Hu, H. Liu, C. Fang, C. Li, F. Xhyliu, H. Dysert, J. Bodo, G. Habermehl, B.E. Russell, W. Li, M. Chappell, X. Jiang, S.L. Ondrejka, E.D. Hsi, J.P. Maciejewski, Q. Yi, K.C. Anderson, N.C. Munshi, G. Ao, J.N. Valent, J. Lin, J. Zhao, Targeting of CD38 by the tumor suppressor miR-26a serves as a novel potential therapeutic agent in multiple myeloma, Cancer Res. 2020, canres.1077.2019.

[2] A.L. Antaris, J.T. Robinson, O.K. Yaghi, G. Hong, S. Diao, R. Luong, H. Dai, Ultra-Low Doses of Chirality Sorted (6,5) Carbon Nanotubes for Simultaneous Tumor Imaging and Photothermal Therapy, ACS Nano. 2013, 7(4) 3644–3652.

[3] C.W. Lin, R.B. Weisman, In vivo detection of single-walled carbon nanotubes: Progress and challenges, Nanomedicine. 2016, 11 (22) 2885–2888.

[4] T.V. Galassi, P.V. Jena, J. Shah, G. Ao, E. Molitor, Y. Bram, A. Frankel, J. Park, J. Jessurun, D.S. Ory, A. Haimovitz-Friedman, D. Roxbury, J. Mittal, M. Zheng, R.E. Schwartz, D.A. Heller, An optical nanoreporter of endolysosomal lipid accumulation reveals enduring effects of diet on hepatic macrophages in vivo, Sci. Transl. Med. 2018, 10 (461) eaar2680.

[5] J.D. Harvey, P. V Jena, H.A. Baker, G.H. Zerze, R.M. Williams, T. V Galassi, D. Roxbury, J. Mittal, D.A. Heller, A carbon nanotube reporter of microRNA hybridization events in vivo, Nat. Biomed. Eng. 2017, 1 0041.

[6] A. Krishnan, E. Dujardin, T.W. Ebbesen, P.N. Yianilos, M.M.J. Treacy, Young's modulus of single-walled nanotubes, Phys. Rev. B. 1998, 58 (20) 14013–14019.

[7] S. Berciaud, L. Cognet, P. Poulin, R.B. Weisman, B. Lounis, Absorption spectroscopy of individual single-walled carbon nanotubes, Nano Lett. 2007, 7 (5) 1203–1207.

[8] J. Chen, V. Perebeinos, M. Freitag, J. Tsang, Q. Fu, J. Liu, P. Avouris, Bright infrared emission from electrically induced excitons in carbon nanotubes, Science. 2005, 310 (5751) 1171–1174.

[9] M.J. O'Connell, S.M. Bachilo, C.B. Huffman, V.V. Moore, M.S. Strano, E.H. Hatoz, K.L. Rialon, P.J. Boul, W.H. Noon, C. Kittrell, J. Ma, R.H. Hague, R.B. Weisman, R.E. Smalley, Band gap fluorescence from individual single-walled carbon nanotubes, Science. 2002, 297 (5581) 593–596.

[10] M. Chehelamirani, M.C. da Silva, D.R. Salahub, Electronic properties of carbon nanotubes complexed with a DNA nucleotide, Phys. Chem. Chem. Phys. 2017, 19 7333–7342.

[11] P.W. Barone, S. Baik, D.A. Heller, M.S. Strano, Near-infrared optical sensors based on single-walled carbon nanotubes, Nat. Mater. 2004, 4 (1) 86–92.

[12] N.M. Iverson, P.W. Barone, M. Shandell, L.J. Trudel, S. Sen, F. Sen, V. Ivanov, E. Atolia, E. Farias, T.P. McNicholas, others, In vivo biosensing via tissue-localizable near-infrared-fluorescent single-walled carbon nanotubes, Nat. Nano. 2013, 8 (11) 873–880.

[13] D. Roxbury, P. V Jena, R.M. Williams, B. Enyedi, P. Niethammer, S. Marcet, M. Verhaegen, S. Blais-Ouellette, D.A. Heller, Hyperspectral microscopy of near-infrared fluorescence enables 17-chirality carbon nanotube imaging, Sci. Rep. 2015, 5 14167.

[14] S. Diao, G. Hong, J.T. Robinson, L. Jiao, A.L. Antaris, J.Z. Wu, C.L. Choi, H. Dai, Chirality enriched (12, 1) and (11, 3) single-walled carbon nanotubes for biological imaging, J. Am. Chem. Soc. 2012, 134 (41) 16971–16974.

[15] L. Ceppi, N.M. Bardhan, Y. Na, A. Siegel, N. Rajan, R. Fruscio, M.G. Del Carmen, A.M. Belcher, M.J. Birrer, Real-time single-walled carbon nanotube-based fluorescence imaging improves survival after debulking surgery in an ovarian cancer model, ACS Nano. 2019, 13 (5) 5356–5365.

[16] S. Kruss, M.P. Landry, E. Vander Ende, B.M.A. Lima, N.F. Reuel, J. Zhang, J. Nelson, B. Mu, A. Hilmer, M. Strano, Neurotransmitter detection using corona phase molecular recognition on fluorescent single-walled carbon nanotube sensors, J. Am. Chem. Soc. 2014, 136 (2) 713–724.

[17] J. Zhang, M.P. Landry, P.W. Barone, J.-H. Kim, S. Lin, Z.W. Ulissi, D. Lin, B. Mu, A.A. Boghossian, A.J. Hilmer, Molecular recognition using corona phase complexes made of synthetic polymers adsorbed on carbon nanotubes, Nat. Nano. 2013, 8 (12) 959.

[18] G. Bisker, J. Dong, H.D. Park, N.M. Iverson, J. Ahn, J.T. Nelson, M.P. Landry, S. Kruss, M.S. Strano, Protein-targeted corona phase molecular recognition, Nat. Commun. 2016, 7 10241.

[19] T. Shiraki, H. Onitsuka, T. Shiraishi, N. Nakashima, Near infrared photoluminescence modulation of single-walled carbon nanotubes based on a molecular recognition approach, Chem. Commun. 2016, 52 12972–12975.

[20] T.V. Galassi, M. Antman-Passig, Z. Yaari, J. Jessurun, R.E. Schwartz, D.A. Heller, Long-term *in vivo* biocompatibility of single-walled carbon nanotubes, PLoS ONE, 2019, 15(5) e0226791.

[21] M. Kim, X. Wu, G. Ao, X. He, H. Kwon, N.F. Hartmann, M. Zheng, S.K. Doorn, Y. Wang, Mapping structure-property relationships of organic color centers, Chem. 2018, 4 (9) 2180–2191.

[22] P. Avouris, M. Freitag, V. Perebeinos, Carbon-nanotube photonics and optoelectronics, Nat. Photon. 2008, 2 341–350.

[23] Y. Miyauchi, M. Iwamura, S. Mouri, T. Kawazoe, M. Ohtsu, K. Matsuda, Brightening of excitons in carbon nanotubes on dimensionality modification, Nat. Photon. 2013, 7 (9) 715–719.

[24] X. He, N.F. Hartmann, X. Ma, Y. Kim, R. Ihly, J.L. Blackburn, W. Gao, J. Kono, Y. Yomogida, A. Hirano, T. Tanaka, H. Kataura, H. Htoon, S.K. Doorn, Tunable room-temperature single-photon emission at telecom wavelengths from sp 3 defects in carbon nanotubes, Nat. Photonics. 2017, 11 (9) 577.

[25] Y. Piao, B. Meany, L.R. Powell, N. Valley, H. Kwon, G.C. Schatz, Y. Wang, Brightening of carbon nanotube photoluminescence through the incorporation of sp3 defects, Nat. Chem. 2013, 5 (10) 840–845.

[26] L.R. Powell, Y. Piao, Y. Wang, Optical Excitation of Carbon Nanotubes Drives Localized Diazonium Reactions, J. Phys. Chem. Lett. 2016, 7 (18) 3690–3694.

[27] F.J. Berger, J. Lüttgens, T. Nowack, T. Kutsch, S. Lindenthal, L. Kistner, C.C. Müller, L.M. Bongartz, V.A. Lumsargis, Y. Zakharko, J. Zaumseil, Brightening of

long, polymer-wrapped carbon nanotubes by sp^3 functionalization in organic solvents, ACS Nano. 2019, 13 (8) 9259–9269.

[28] C.F. Chiu, W.A. Saidi, V.E. Kagan, A. Star, Defect-induced near-infrared photoluminescence of single-walled carbon nanotubes treated with polyunsaturated fatty acids, J. Am. Chem. Soc. 2017, 139 (13) 4859–4865.

[29] Y. Iizumi, M. Yudasaka, J. Kim, H. Sakakita, T. Takeuchi, T. Okazaki, Oxygen-doped carbon nanotubes for near-infrared fluorescent labels and imaging probes, Sci Rep. 2018, 8, 6272.

[30] C.-W. Lin, S.M. Bachilo, Y. Zheng, U. Tsedev, S. Huang, R.B. Weisman, A.M. Belcher, Creating fluorescent quantum defects in carbon nanotubes using hypochlorite and light, Nat. Commun. 2019, 10, 2874.

[31] D. Roxbury, X. Tu, M. Zheng, A. Jagota, Recognition ability of DNA for carbon nanotubes correlates with their binding affinity, Langmuir. 2011, 27 (13) 8282–8293.

[32] A. Shankar, J. Mittal, A. Jagota, Binding between DNA and carbon nanotubes strongly depends upon sequence and chirality, Langmuir. 2014, 30 (11) 3176–3183.

[33] Y. Kato, A. Inoue, Y. Niidome, N. Nakashima, Thermodynamics on soluble carbon nanotubes: How do DNA molecules replace surfactants on carbon nanotubes?, Sci. Rep. 2012, 2, 1–7.

[34] A. Shankar, M. Zheng, A. Jagota, Energetic basis of single wall carbon nanotube enantiomer recognition by single stranded DNA, J. Phys. Chem. C. 2017, 121 (32) 17479–17487.

[35] K.R. Hinkle, F.R. Phelan, Solvation of carbon nanoparticles in water/alcohol mixtures: using molecular simulation to probe energetics, structure, and dynamics, J. Phys. Chem. C. 2017, 121 (41) 22926–22938.

[36] D. Roxbury, A. Jagota, J. Mittal, Structural characteristics of oligomeric dna strands adsorbed onto single-walled carbon nanotubes, J. Phys. Chem. B. 2017, 117 (1) 132–140.

[37] D. Roxbury, A. Jagota, J. Mittal, Sequence-specific self-stitching motif of short single-stranded DNA on a single-walled carbon nanotube, J. Am. Chem. Soc. 2011, 133, 13545–13550.

[38] Y. Yang, M. Zheng, A. Jagota, Learning to predict single-wall carbon nanotube-recognition DNA sequences, Npj Comp. Mat. 2019, 5, 3.

[39] X. Chen, G.S. Lee, A. Zettl, C.R. Bertozzi, Biomimetic engineering of carbon nanotubes by using cell surface mucin mimics, Angew. Chem. Int. Ed. 2004, 43 (45) 6111–6116.

[40] S. Iijima, Helical microtubules of graphitic carbon, Nature. 1991, 354, 56–58.

[41] D.S. Bethune, C.H. Kiang, M.S. de Vries, G. Gorman, R. Savoy, J. Vazquez, R. Beyers, Cobalt-catalysed growth of carbon nanotubes with single-atomic-layer walls, Nature. 1993, 363, 605–607.

[42] T. Guo, P. Nikolaev, A. Thess, D.T. Colbert, R.E. Smalley, Catalytic growth of single-walled manotubes by laser vaporization, Chem. Phys. Lett. 21995, 43, 49–54.

[43] A.E. Agboola, R.W. Pike, T.A. Hertwig, H.H. Lou, Conceptual design of carbon nanotube processes, Clean Techn. Environ. Policy. 2007, 9, 289–311.

[44] P. Nikolaev, M.J. Bronikowski, R.K. Bradley, F. Rohmund, D.T. Colbert, K.A. Smith, R.E. Smalley, Gas-phase catalytic growth of single-walled carbon nanotubes from carbon monoxide, Chem. Phys. Lett. 1999, 313, 91–97.

[45] M.J. Bronikowski, P.A. Willis, D.T. Colbert, K.A. Smith, R.E. Smalley, Gas-phase production of carbon single-walled nanotubes from carbon monoxide via the HiPco process: A parametric study, J. Vac. Sci. Tech. A. 2001, 19 1800–1805.

[46] D.E. Resasco, W.E. Alvarez, F. Pompeo, L. Balzano, J.E. Herrera, B. Kitiyanan, A. Borgna, A scalable process for production of single-walled carbon nanotubes (SWCNTs) by catalytic disproportionation of CO on a solid catalyst, J. of Nano. Res. 2002, 4, 131–136.

[47] J. Lee, D.-M. Lee, Y.-K. Kim, H.S. Jeong, S.M. Kim, Significantly Increased Solubility of carbon nanotubes in superacid by oxidation and their assembly into high-performance fibers, Small. 2017, 13, 1701131.

[48] P. Wang, M. Kim, Z. Peng, C.-F. Sun, J. Mok, A. Lieberman, Y. Wang, Superacid-surfactant exchange: enabling nondestructive dispersion of full-length carbon nanotubes in water, ACS Nano. 2017, 11, 9231–9238.

[49] L.A. Girifalco, M. Hodak, R.S. Lee, Carbon nanotubes, buckyballs, ropes, and a universal graphitic potential, Phys. Rev. B. 2000, 62 13104–13110.

[50] S. Saitō, A.K. Zettl, eds., Optical spectroscopy of single-walled carbon nanotubes, in: Carbon Nanotubes: Quantum Cylinders of Graphene, Elsevier, Amsterdam, The Netherlands, 2008: pp. 109–133.

[51] B. Wu, D. Geng, Y. Liu, Evaluation of metallic and semiconducting single-walled carbon nanotube characteristics, Nanoscale. 2011, 3, 2074–2085.

[52] J.-C. Charlier, X. Blase, S. Roche, Electronic and transport properties of nanotubes, Rev. Mod. Phys. 2007, 79 (2) 677–732.

[53] M. Zheng, J.A. Fagan, Particles, Tubes, and Colloids, n.d. https://www.nist.gov/programs-projects/particles-tubes-and-colloids (accessed July 13, 2020).

[54] D.A. Walters, L.M. Ericson, M.J. Casavant, J. Liu, D.T. Colbert, K.A. Smith, R.E. Smalley, Elastic strain of freely suspended single-wall carbon nanotube ropes, Appl. Phys. Lett. 1999, 74, 3803–3805.

[55] M.-F. Yu, B.S. Files, S. Arepalli, R.S. Ruoff, Tensile loading of ropes of single wall carbon nanotubes and their mechanical properties, Phys. Rev. Lett. 2000, 84, 5552–5555.

[56] H.M. Duong, E. Einarsson, J. Okawa, R. Xiang, S. Maruyama, Thermal degradation of single-walled carbon nanotubes, Jpn. J. Appl. Phys. 2008, 47, 1994–1999.

[57] G. Hong, S. Diao, J. Chang, A.L. Antaris, C. Chen, B. Zhang, S. Zhao, D.N. Atochin, P.L. Huang, K.I. Andreasson, C.J. Kuo, H. Dai, Through-skull fluorescence imaging of the brain in a new near-infrared window, Nature Photon. 2014, 8, 723–730.

[58] T.K. Leeuw, R.M. Reith, R.A. Simonette, M.E. Harden, P. Cherukuri, D.A. Tsyboulski, K.M. Beckingham, R.B. Weisman, Single-walled carbon nanotubes in the intact organism: Near-IR imaging and biocompatibility studies in Drosophila, Nano Lett. 2007, 7, 2650–2654.

[59] F. Wang, G. Dukovic, L.E. Brus, T.F. Heinz, The optical resonances in carbon nanotubes arise from excitons, Science. 2005, 308 (5723) 838–841.

[60] J. Lefebvre, P. Finnie, Excited excitonic states in single-walled carbon nanotubes, Nano Lett. 2008, 8 (7) 1890–1895.

[61] M. Zheng, A. Jagota, E.D. Semke, B.A. Diner, R.S. Mclean, S.R. Lustig, R.E. Richardson, N.G. Tassi, DNA-assisted dispersion and separation of carbon nanotubes, Nat. Mat. 2003, 2, 338–342.

[62] M. Zheng, A. Jagota, M.S. Strano, A.P. Santos, P. Barone, S.G. Chou, B.A. Diner, M.S. Dresselhaus, R.S. McLean, G.B. Onoa, G.G. Samsonidze, E.D. Semke, M. Usrey, D.J. Walls, Structure-based carbon nanotube sorting by sequence-dependent DNA assembly, Science. 2003, 302 (5650) 1545–1548.

[63] X. Tu, S. Manohar, A. Jagota, M. Zheng, DNA sequence motifs for structure-specific recognition and separation of carbon nanotubes, Nature. 2009, 460, 250–253.

[64] M. Zheng, Sorting carbon nanotubes, Top. Curr. Chem. 2017, 375 (1) 13.

[65] G. Ao, J.K. Streit, J.A. Fagan, M. Zheng, Differentiating left- and right-handed carbon nanotubes by DNA, J. Am. Chem. Soc. 2016, 138, 16677–16685.

[66] G. Ao, C.Y. Khripin, M. Zheng, DNA-controlled partition of carbon nanotubes in polymer aqueous two-phase systems, J. Am. Chem. Soc. 2014, 136 (29) 10383–10392.

[67] R.B. Weisman, Chapter 5 Optical spectroscopy of single-walled carbon nanotubes, Contemp. Conc. Cond. Matt. Sci., Elsevier, 2008: pp. 109–133.

[68] R.B. Weisman, S.M. Bachilo, Dependence of optical transition energies on structure for single-walled carbon nanotubes in aqueous suspension: an empirical kataura plot, Nano Lett. 2003, 3 (9) 1235–1238.

[69] B.A. Larsen, P. Deria, J.M. Holt, I.N. Stanton, M.J. Heben, M.J. Therien, J.L. Blackburn, Effect of solvent polarity and electrophilicity on quantum yields and solvatochromic shifts of single-walled carbon nanotube photoluminescence, J. Am. Chem. Soc. 2012, 134 (30) 12485–12491.

[70] F.F. Bergler, F. Schöppler, F.K. Brunecker, M. Hailman, T. Hertel, Fluorescence spectroscopy of gel-immobilized single-wall carbon nanotubes with microfluidic control of the surfactant environment, J. Phys. Chem. C. 2013, 117, 13318–13323.

[71] J.H. Choi, M.S. Strano, Solvatochromism in single-walled carbon nanotubes, Appl. Phys. Lett. 2007, 90, 22314.

[72] K. Yum, J.-H. Ahn, T.P. McNicholas, P.W. Barone, B. Mu, J.-H. Kim, R.M. Jain, M.S. Strano, Boronic acid library for selective, reversible near-infrared fluorescence quenching of surfactant suspended single-walled carbon nanotubes in response to glucose, Acs Nano. 2011, 6, 819–830.

[73] R. Rastogi, R. Kaushal, S.K. Tripathi, A.L. Sharma, I. Kaur, L.M. Bharadwaj, Comparative study of carbon nanotube dispersion using surfactants, J. Colloid Int. Sci. 2008, 328, 421–428.

[74] X. Gong, J. Liu, S. Baskaran, R.D. Voise, J.S. Young, Surfactant-assisted processing of carbon nanotube/polymer composites, Chem. Mater. 2000, 12 (4) 1049–1052.

[75] I.H. Hafez, M.R. Berber, T. Fujigaya, N. Nakashima, Enhancement of platinum mass activity on the surface of polymer-wrapped carbon nanotube-based fuel cell electrocatalysts, Sci Rep. 2015, 4, 6295.

[76] H. Dohi, S. Kikuchi, S. Kuwahara, T. Sugai, H. Shinohara, Synthesis and spectroscopic characterization of single-wall carbon nanotubes wrapped by glycoconjugate polymer with bioactive sugars, Chem. Phys. Lett. 2006, 428 (1) 98–101.

[77] E.T. Mickelson, C.B. Huffman, A.G. Rinzler, R.E. Smalley, R.H. Hauge, J.L. Margrave, Fluorination of single-wall carbon nanotubes, Chem. Phys. Lett. 1998, 296, 188–194.

[78] L. Cognet, D.A. Tsyboulski, J.-D.R. Rocha, C.D. Doyle, J.M. Tour, R.B. Weisman, Stepwise quenching of exciton fluorescence in carbon nanotubes by single-molecule reactions, Science. 2007, 316, 1465–1468.

[79] S.M. Bachilo, Structure-assigned optical spectra of single-walled carbon nanotubes, Science. 2002, 298, 2361–2366.

[80] Y.-Z. Ma, L. Valkunas, S.L. Dexheimer, S.M. Bachilo, G.R. Fleming, Femtosecond spectroscopy of optical excitations in single-walled carbon nanotubes: evidence for exciton-exciton annihilation, Phys. Rev. Lett. 2005, 94, 157402.

[81] T. Hertel, S. Himmelein, T. Ackermann, D. Stich, J. Crochet, Diffusion limited photoluminescence quantum yields in 1-D semiconductors: single-wall carbon nanotubes, ACS Nano. 2010, 4 (12) 7161–7168.

[82] B.E. Collins, J.C. Paulson, Cell surface biology mediated by low affinity multivalent protein–glycan interactions, Curr. Opinion Chem. Bio. 2004, 8 (6) 617–625.

[83] A.L. Parry, N.A. Clemson, J. Ellis, S.S.R. Bernhard, B.G. Davis, N.R. Cameron, 'Multicopy multivalent' glycopolymer-stabilized gold nanoparticles as potential synthetic cancer vaccines, J. Am. Chem. Soc. 2013, 135 (25) 9362–9365.

[84] A.P.P. Kröger, M.I. Komil, N.M. Hamelmann, A. Juan, M.H. Stenzel, J.M.J. Paulusse, Glucose single-chain polymer nanoparticles for cellular targeting, ACS Macro Lett. 2019, 8, 95–101.

[85] H. Zhang, Y. Ma, X.-L. Sun, Recent developments in carbohydrate-decorated targeted drug/gene delivery, Med. Res. Rev. 2009, 30 (2) 270-289.

[86] Thermo Fisher, Photoreactive Crosslinker Chemistry: Aryl azide reaction chemistry, (n.d.) Accessed July 30, 2020.

[87] L.-H. Liu, M. Yan, Perfluorophenyl azides: new applications in surface functionalization and nanomaterial synthesis, Acc. Chem. Res. 2010, 43, 1434–1443.

[88] N. Kong, M.R. Shimpi, O. Ramström, M. Yan, Carbohydrate conjugation through microwave-assisted functionalization of single-walled carbon nanotubes using perfluorophenyl azides, Carbohydr. Res. 2015, 405, 33–38.

[89] L. Xu, J. Farrell, R.G. Karunakaran, A. Honglawan, S. Yang, Synthesis of dual-functional copolymer with orthogonally photosensitive groups, J. Polym. Sci. A Polym. Chem. 2013, 51, 1215–1222.

[90] J. Baier, T. Maisch, M. Maier, M. Landthaler, W. Bäumler, Direct detection of singlet oxygen generated by UVA irradiation in human cells and skin, J. Invest. Derma. 2007, 127 (6) 1498–1506.

[91] Z. Farooq, D.A. Chestakov, B. Yan, G.C. Groenenboom, W.J. van der Zande, D.H. Parker, Photodissociation of singlet oxygen in the UV region, Phys. Chem. Chem. Phys. 2014, 16, 3305–3316.

[92] Y. Zheng, S.M. Bachilo, R.B. Weisman, Quenching of single-walled carbon nanotube fluorescence by dissolved oxygen reveals selective single-stranded DNA affinities, J. Phys. Chem. Lett. 2017, 8, 1952–1955.

[93] D.A. Heller, H. Jin, B.M. Martinez, D. Patel, B.M. Miller, T.-K. Yeung, P. V Jena, C. Höbartner, T. Ha, S.K. Silverman, others, Multimodal optical sensing and analyte specificity using single-walled carbon nanotubes, Nature Nano. 2009, 4, 114–120.

[94] X. Ma, L.-H. Zhang, L.-R. Wang, X. Xue, J.-H. Sun, Y. Wu, G. Zou, X. Wu, P.C. Wang, W.G. Wamer, Single-walled carbon nanotubes alter cytochrome c electron transfer and modulate mitochondrial function, ACS Nano. 2012, 6, 10486–10496.

[95] N. Yang, X. Jiang, Nanocarbons for DNA sequencing: A review, Carbon. 2017, 115, 293–311.

[96] Y. Yomogida, T. Tanaka, M. Zhang, M. Yudasaka, X. Wei, H. Kataura, Industrial-scale separation of high-purity single-chirality single-wall carbon nanotubes for biological imaging, Nature Commun. 2016, 7, 12056.

[97] Md.T. Hasan, E. Campbell, O. Sizova, V. Lyle, G. Akkaraju, D.L. Kirkpatrick, A. V. Naumov, Multi-drug/gene NASH therapy delivery and selective hyperspectral NIR imaging using chirality-sorted single-walled carbon nanotubes, Cancers. 2019, 11 (18) 1175.

[98] J.P. Giraldo, M.P. Landry, S.Y. Kwak, R.M. Jain, M.H. Wong, N.M. Iverson, M. Ben-Naim, M.S. Strano, A ratiometric sensor using single chirality near-infrared fluorescent carbon nanotubes: application to in vivo monitoring, Small. 2015, 11 (32) 3973–3984.

[99] R.L. Pinals, D. Yang, A. Lui, W. Cao, M.P. Landry, Corona exchange dynamics on carbon nanotubes by multiplexed fluorescence monitoring, J. Am. Chem. Soc. 2020, 142 (3) 1254–1264.

[100] A. Saha, B.J. Gifford, X. He, G. Ao, M. Zheng, H. Kataura, H. Htoon, S. Kilina, S. Tretiak, S.K. Doorn, Narrow-band single-photon emission through selective aryl functionalization of zigzag carbon nanotubes, Nature Chemistry. 2018, 10, 1089–1095.

[101] Y. Yang, A. Shankar, T. Aryaksama, M. Zheng, A. Jagota, Quantification of DNA/SWCNT solvation differences by aqueous two-phase separation, Langmuir. 2018, 34 (5) 1834–1843.

[102] R.R. Johnson, A.T. Johnson, M.L. Klein, The nature of DNA-base–carbon-nanotube interactions, Small. 2010, 6, 31–34.

[103] Y. Zheng, S.M. Bachilo, R.B. Weisman, Controlled patterning of carbon nanotube energy levels by covalent DNA functionalization, ACS Nano. 2019, 13, 8222–8228.

[104] M. Gravely, M.M. Safaee, D. Roxbury, Biomolecular functionalization of a nanomaterial to control stability and retention within live cells, Nano Lett. 2019, 19 (9) 6203–6212.

[105] R.R. Johnson, A.T.C. Johnson, M.L. Klein, Probing the structure of DNA−carbon nanotube hybrids with molecular dynamics, Nano Lett. 2008, 8 (1) 69–75.

[106] S. Iliafar, J. Mittal, D. Vezenov, A. Jagota, Interaction of single-stranded DNA with curved carbon nanotube is much stronger than with flat graphite, J. Am. Chem. Soc. 2014, 136 (37) 12947–12957.

[107] Y. Zheng, S.M. Bachilo, R.B. Weisman, Enantiomers of single-wall carbon nanotubes show distinct coating displacement kinetics, J. Phys. Chem. Lett. 2018, 9 (13) 3793–3797.

[108] P. V Jena, M.M. Safaee, D.A. Heller, D. Roxbury, DNA-carbon nanotube complexation affinity and photoluminescence modulation are independent, ACS Appl. Mat. Int. 2017, 9 (25) 21397–21405.

[109] G. Ao, M. Zheng, Preparation and separation of DNA-wrapped carbon nanotubes, Curr. Prot. Chem. Bi. 2015, 7 (1) 43–51.

[110] C.Y. Khripin, N. Arnold-Medabalimi, M. Zheng, Molecular-crowding-induced clustering of DNA-wrapped carbon nanotubes for facile length fractionation, ACS Nano. 2011, 5 (10) 8258–8266.

[111] M. Zheng, B.A. Diner, Solution redox chemistry of carbon nanotubes, J. Am. Chem. Soc. 2004, 126 (47) 15490–15494.

[112] A.R.T. Nugraha, R. Saito, K. Sato, P.T. Araujo, A. Jorio, M.S. Dresselhaus, Dielectric constant model for environmental effects on the exciton energies of single wall carbon nanotubes, Appl. Phys. Lett. 2010, 97, 091905.

[113] D.A. Tsyboulski, E.L. Bakota, L.S. Witus, J.-D.R. Rocha, J.D. Hartgerink, R.B. Weisman, Self-assembling peptide coatings designed for highly luminescent suspension of single-walled carbon nanotubes, J. Am. Chem. Soc. 2008, 130 (50) 17134–17140.

[114] X. Gong, A.K. Sharma, M.S. Strano, D. Mukhopadhyay, Selective assembly of DNA-conjugated single-walled carbon nanotubes from the vascular secretome, ACS Nano. 2014, 8 (9) 9126–9136.

[115] Y. Yang, A. Sharma, G. Noetinger, M. Zheng, A. Jagota, Pathway-dependent structures of DNA-wrapped carbon nanotubes: direct sonication vs surfactant/DNA exchange, J. Phys. Chem. C. 2020, 124 (16) 9045–9055.

[116] J.K. Streit, J.A. Fagan, M. Zheng, A low energy route to DNA-wrapped carbon nanotubes via replacement of bile salt surfactants, Analytical Chemistry. 2017, 89 (19) 10496–10503.

[117] S. Ghosh, S.M. Bachilo, R.A. Simonette, K.M. Beckingham, R.B. Weisman, Oxygen doping modifies near-infrared band gaps in fluorescent single-walled carbon nanotubes, Science. 2010, 330 (6011) 1656–1659.

[118] J. Chen, R. Dhall, B. Hou, S. Yang, B. Wang, D. Kang, S.B. Cronin, Enhanced photoluminescence in air-suspended carbon nanotubes by oxygen doping, Appl. Phys. Lett. 2016, 109, 153109.

[119] X. Ma, L. Adamska, H. Yamaguchi, S.E. Yalcin, S. Tretiak, S.K. Doorn, H. Htoon, Electronic structure and chemical nature of oxygen dopant states in carbon nanotubes, ACS Nano. 2014, 8 (10) 10782–10789.

[120] M.S. Hofmann, J.T. Glückert, J. Noé, C. Bourjau, R. Dehmel, A. Högele, Bright, long-lived and coherent excitons in carbon nanotube quantum dots, Nature Nanotech. 2013, 8 (7) 502–505.

[121] X. Ma, N.F. Hartmann, J.K.S. Baldwin, S.K. Doorn, H. Htoon, Room-temperature single-photon generation from solitary dopants of carbon nanotubes, Nature Nanotech. 2015, 10 (8) 671–675.

[122] X. He, K.A. Velizhanin, G. Bullard, Y. Bai, J.-H. Olivier, N.F. Hartmann, B.J. Gifford, S. Kilina, S. Tretiak, H. Htoon, M.J. Therien, S.K. Doorn, Solvent- and

wavelength-dependent photoluminescence relaxation dynamics of carbon nanotube sp ^{3} defect states, ACS Nano. 2018, 12 (8) 8060–8070.

[123] J. Tang, E. Ozhegov, Y. Liu, D. Wang, X. Yao, X.-L. Sun, Straightforward synthesis of n-glycan polymers from free glycans via cyanoxyl free radical-mediated polymerization, ACS Mac. Lett. 2017, 6 (2) 107–111.

[124] K.K. Chan, Q. Shi, J. Tang, X.-L. Sun, Synthesis of aryl azide chain-end functionalized N-linked gcan polymer and its photo-labeling of specific proteins, ACS Mac. Lett. (n.d.) Submitted.

[125] Y. Zheng, S.M. Bachilo, R.B. Weisman, Quenching of single-walled carbon nanotube fluorescence by dissolved oxygen reveals selective single-stranded DNA affinities, J. Phys. Chem. Lett. 2017, 8 (9) 1952–1955.

Appendix A

Supplementary Data

Chirality-Pure Carbon Nanotubes Show Distinct Complexation with Recognition DNA Sequences

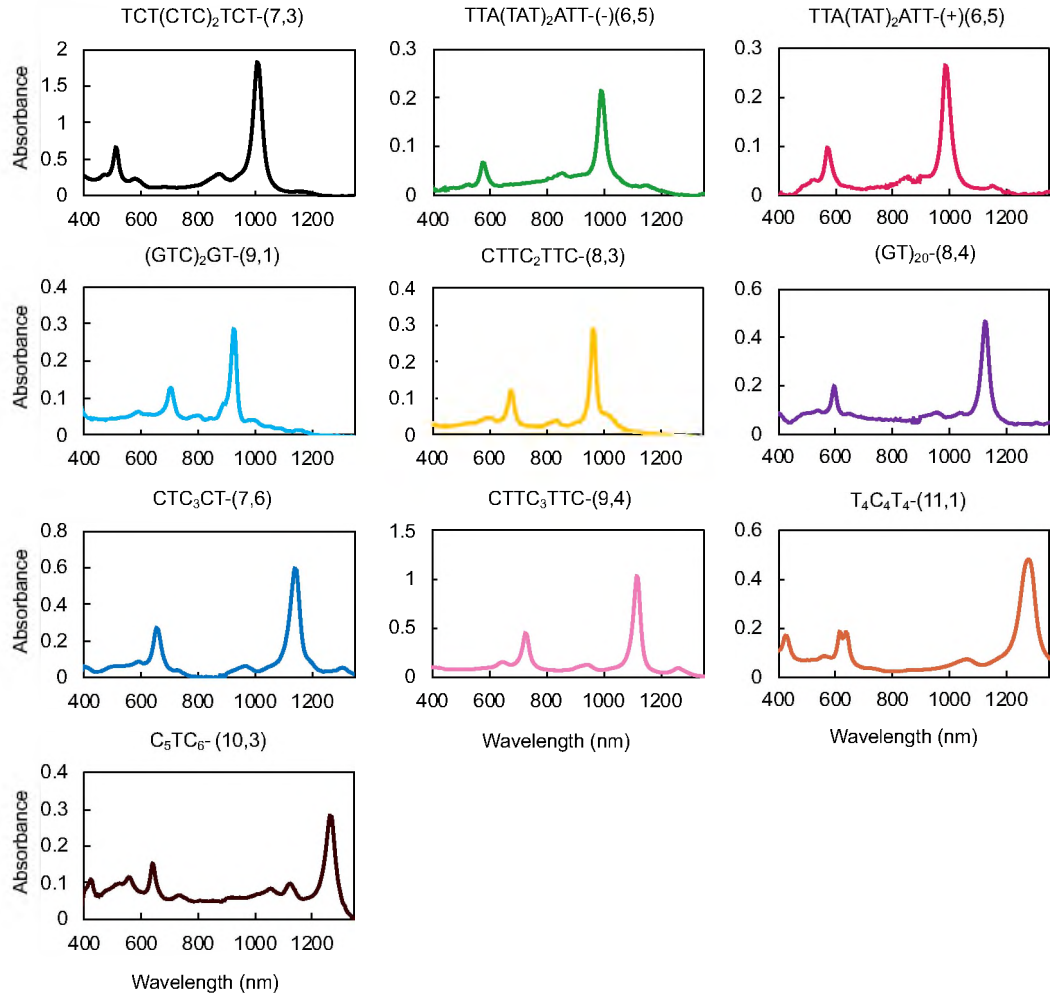

Figure 1. Absorbance spectra of DNA-wrapped (*n, m*) SWCNT species purified by polymer aqueous-two phase separation method.

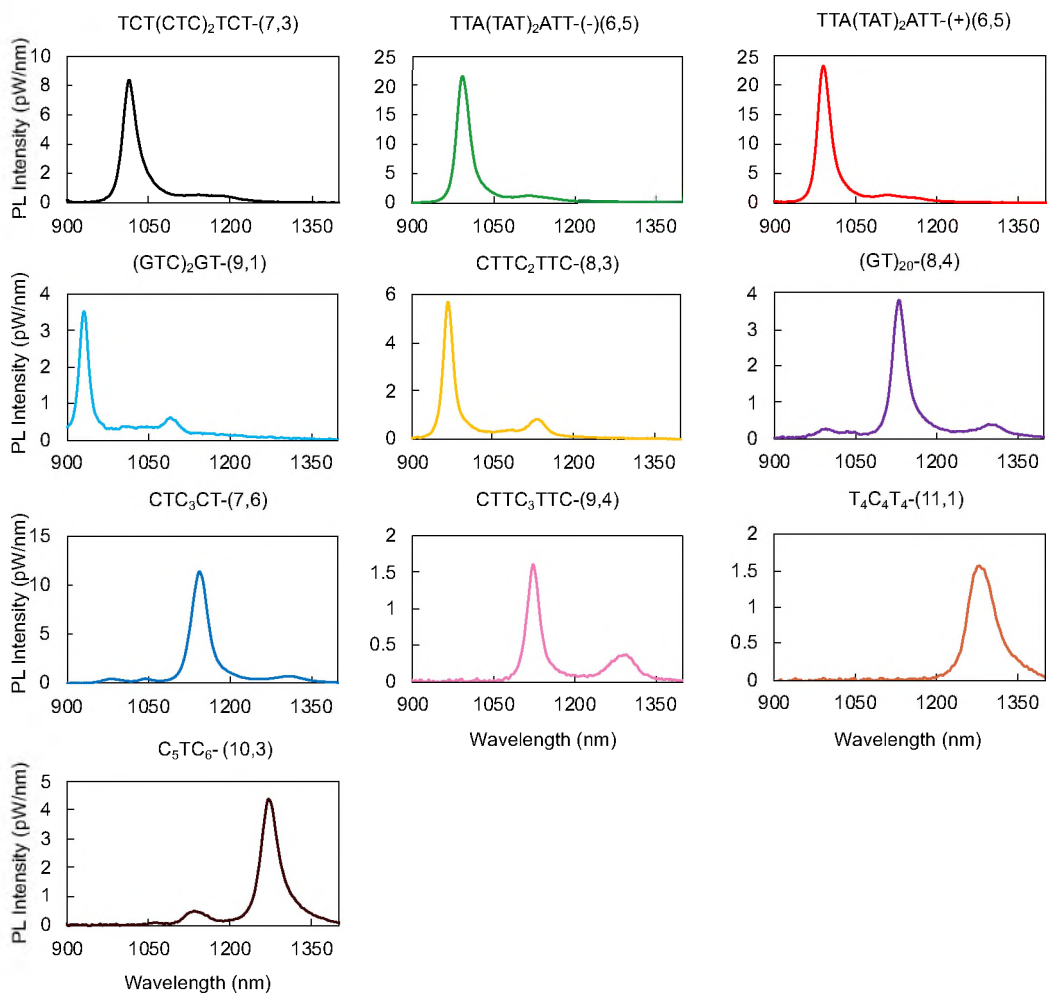

Figure 2. Fluorescence spectra of DNA-wrapped (*n, m*) SWCNT species purified by polymer aqueous-two phase separation method. All nanotube samples were excited at the E_{22} peak wavelength of (*n, m*) species.

Table 1. List of pure-chirality (n, m) SWCNT wrapped by DNA recognition sequences and the corresponding absorption wavelength shift at the E11 peak positions of DNA- and SDC-coated (n, m) SWCNTs at equilibrium.

DNA-SWCNT	DNA-(n, m) SWCNT λ_{11} (nm)	SDC-(n, m) SWCNT λ_{11} (nm)	$\Delta\lambda_{11}$(nm)
$TCT(CTC)_2TCT$- (7,3)	1009.9±0.0	1001.7±0.0	8.2±0.0
$TTA(TAT)_2ATT$- (+) (6,5)	988.6±0.0	983.6±0.0	5.0±0.0
$TTA(TAT)_2ATT$- (−) (6,5)	991.8±0.0	983.6±0.0	8.2±0.0
$(GTC)_2GT$-(9,1)	927.6±0.0	924.3±0.0	3.3±0.0
$CTTC_2TTC$-(8,3)	963.9±0.0	963.9±0.0	0.0
CTC_3TC-(7,6)	1137.8±0.0	1131.3±0.0	6.5±0.0
$CTTC_3TTC$-(9,4)	1118.7±0.7	1113.8±0.7	4.9±1.3
$T_4C_4T_4$-(11,1)	1273.3±0.3	1264.7±0.0	8.6±0.6
C_5TC_6-(10,3)	1266.3±0.0	1261.5±0.0	4.8±0.0

Table 2. List of pure-chirality (*n, m*) SWCNT wrapped by DNA recognition sequences and the corresponding E_{11} emission features of DNA- and SDC-coated (*n, m*) SWCNTs at equilibrium.

DNA-SWCNT	DNA-(n, m) SWCNT			SDC-(n, m) SWCNT		
	I_O (pW/nm)	λ_{11} (nm)	FWHM (nm)	I_{final} (pW/nm)	λ_{11} (nm)	FWHM (nm)
$TCT(CTC)_2TCT$-(7,3)	7.67±0.97	1013.2±0.0	37.80±0.00	20.57±1.35	1005.0±0.0	26.85±0.78
$TTA(TAT)_2ATT$- (+) (6,5)	22.93±0.33	990.2±0.0	27.96±0.00	36.83±1.27	985.2±0.0	25.22±0.39
$TTA(TAT)_2ATT$- (−) (6,5)	20.00±2.71	995.1±0.0	27.96±0.00	26.20±2.01	985.2±0.0	27.96±0.00
$(GTC)_2GT$-(9,1)	3.14±0.55	929.3±0.0	21.15±0.39	11.67±1.06	926.0±0.0	17.58±0.39
$CTTC_2TTC$-(8,3)	5.32±0.45	965.5±0.0	21.40±0.00	77.70±4.41	965.5±0.0	16.87±0.50
CTC_3TC-(7,6)	8.79±2.96	1142.6±0.0	34.03±0.39	34.20±2.65	1133.9±0.7	26.96±0.67
$CTTC_3TTC$-(9,4)	2.10±0.55	1123.0±0.0	26.16±0.00	25.73±3.11	1116.5±0.0	20.17±0.39
$T_4C_4T_4$-(11,1)	1.60±0.05	1278.7±0.7	56.11±0.38	17.33±0.17	1264.7±0.0	27.55±0.66
C_5TC_6-(10,3)	4.32±0.30	1269.5±0.0	37.25±1.15	10.27±0.81	1263.1±0.0	28.36±0.00

Table 3. List of pure-chirality (*n, m*) SWCNTs wrapped by DNA recognition sequences and the corresponding spectral changes of E_{11} emission peaks after DNA/SDC exchange at equilibrium.

DNA-SWCNT	I/I_0 at equilibrium	$\Delta\lambda_{11}$(nm)	ΔE_{11} (meV)	ΔFWHM (nm)	Laser* (nm)
TCT(CTC)$_2$TCT-(7,3)	2.75±0.54	8.2±0.0	10.0±0.0	10.95±0.77	532
TTA(TAT)$_2$ATT-(+) (6,5)	1.61±0.03	4.9±0.0	6.2±0.0	2.73±0.38	532
TTA(TAT)$_2$ATT-(−) (6,5)	1.32±0.09	9.9±0.0	12.4±0.0	0.01±0.00	532
(GTC)$_2$GT-(9,1)	3.91±1.12	3.3±0.0	4.8±0.0	3.57±0.77	641
CTTC$_2$TTC-(8,3)	14.74±2.07	0	0	4.53±0.50	641
CTC$_3$TC-(7,6)	4.43±1.64	8.7±0.7	8.4±0.3	7.06±0.77	641
CTTC$_3$TTC-(9,4)	12.81±2.74	6.5±0.0	6.4±0.0	5.99±0.38	641
T$_4$C$_4$T$_4$-(11,1)	10.87±0.28	14.0±0.7	11.2±1.5	28.55±0.76	641
C$_5$TC$_6$-(10,3)	2.38±0.03	6.4±0.0	5.0±0.00	8.88±1.14	641

*Fixed excitation wavelengths of 532 and 641 nm lasers correspond to E_{22} peak positions of (*n, m*) SWCNTs.

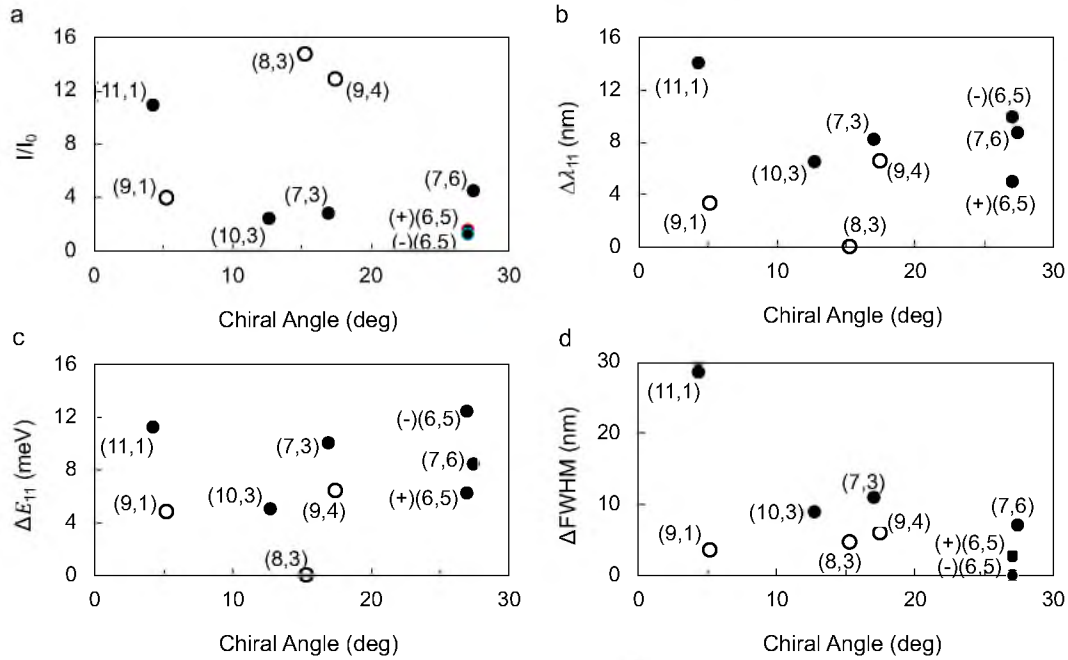

Figure 3. Spectral changes of E_{11} emission peaks of pure-chirality (*n, m*) SWCNT species as a function of nanotube chiral angle after DNA/SDC exchange at equilibrium. (a) PL intensity ratio increase, (b) wavelength and (c) energy shift, and (d) narrowing spectral line width of (*n, m*) species. Closed and open circles indicate mod 1 and mod 2, respectively.

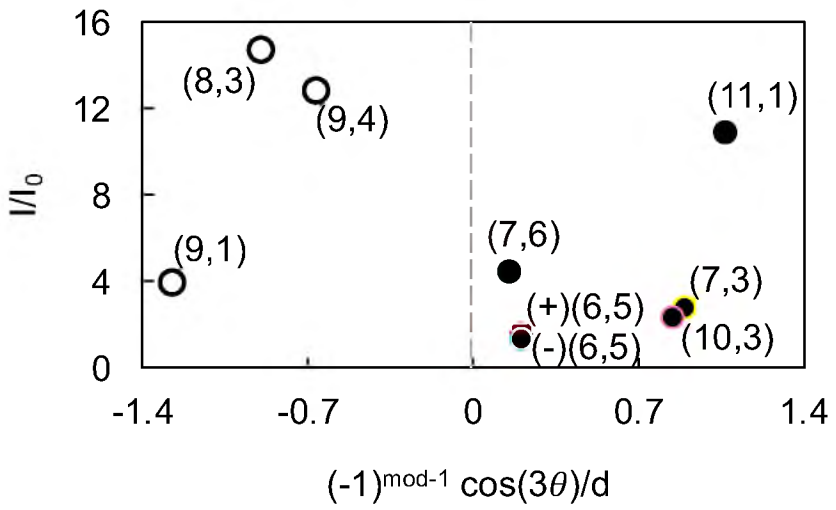

Figure 4. The PL intensity ratio I/Io of E_{11} emission peaks of purified (*n*, *m*) SWCNT species as a function of nanotube chirality (i.e., diameter d and chiral angle θ) after DNA/SDC exchange at equilibrium. The dashed line indicates metallic armchair SWCNTs with the chiral angle θ = 30°. Closed and open circles indicate mod 1 and mod 2, respectively.

Table 4. Exponential fits of E_{11} intensity ratio I/I_O vs. time for surface exchange reaction using $y = a\left(1 - e^{-x/t}\right) + c$. Standard deviations (STDEV) and 95% confidence intervals (CI) were obtained from repeats of three separate samples (i.e., the sample size n = 3).

DNA-SWCNT	a		c		t (s)		R^2	
	STDEV	95% CI	STDEV	95% CI	STDEV	95% CI	STDEV	95% CI
$TCT(CTC)_2TCT$-(7,3)	1.56± 0.15	1.56± 0.38	1.01± 0.01	1.01± 0.02	9.14± 2.01	9.14± 5.01	0.95± 0.01	0.95± 0.02
$TTA(TAT)_2ATT$-(+) (6,5)	0.61± 0.03	0.61± 0.09	0.97± 0.01	0.97± 0.04	18.61± 3.22	18.61± 8.02	0.94± 0.02	0.94± 0.05
$TTA(TAT)_2ATT$-(−) (6,5)	0.35± 0.03	0.35± 0.09	0.95± 0.04	0.95± 0.10	52.43± 2.87	52.43± 7.14	0.91± 0.02	0.91± 0.05
$(GTC)_2GT$-(9,1)	7.37± 1.53	7.37± 3.81	2.17± 1.12	2.17± 2.79	27.54± 4.95	27.54± 12.32	0.94± 0.01	0.94± 0.04
$CTTC_2TTC$-(8,3)	62.50± 2.09	62.50± 5.20	12.88± 0.62	12.88± 1.54	46.19± 1.83	46.19± 4.55	0.97± 0.01	0.97± 0.01
CTC_3TC-(7,6)	26.31± 0.57	26.31± 1.43	8.69± 2.23	8.69± 5.54	230.17 ±31.65	230.17 ±78.63	0.99± 0.00	0.99± 0.01
$CTTC_3TTC$-(9,4)	12.12± 2.49	12.12± 6.19	0.69± 0.50	0.69± 1.25	16.02± 0.19	16.02± 0.49	0.91± 0.01	0.91± 0.03
$T_4C_4T_4$-(11,1)	11.68± 3.00	11.68± 7.45	1.15± 0.15	1.15± 0.39	14.92± 0.95	14.92± 2.37	0.92± 0.04	0.92± 0.11
C_5TC_6-(10,3)	1.35± 0.12	1.35± 0.31	1.03± 0.19	1.03± 0.47	84.62± 27.91	84.62± 69.35	0.97± 0.03	0.97± 0.07

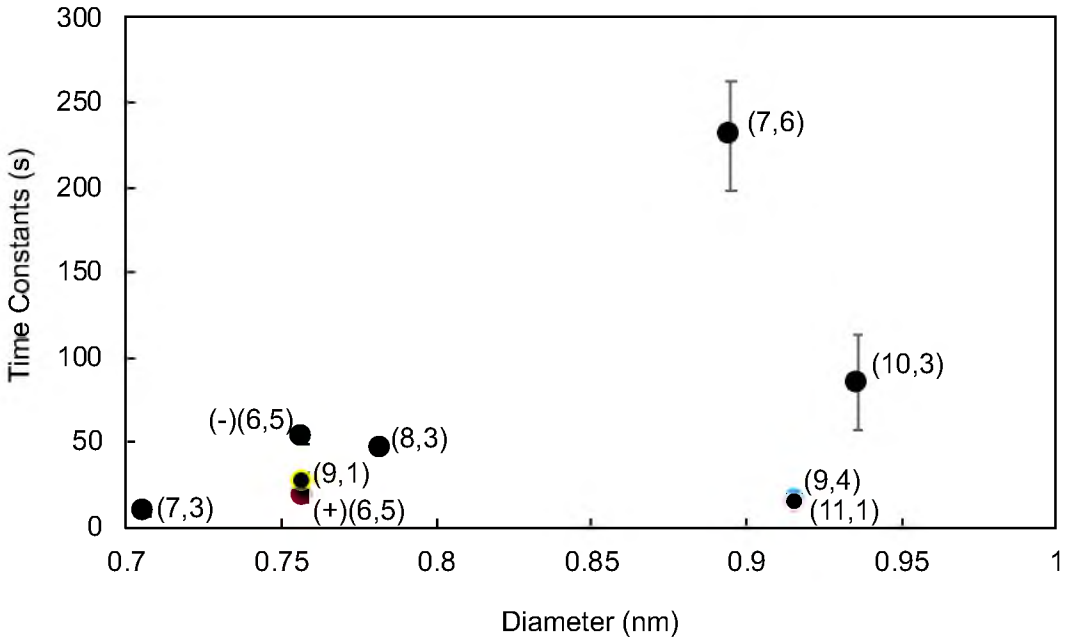

Figure 5. Time constants as a function of nanotube diameter for DNA/SDC displacement on purified (*n, m*) species. The error bars were obtained from the standard deviation of three repeats.

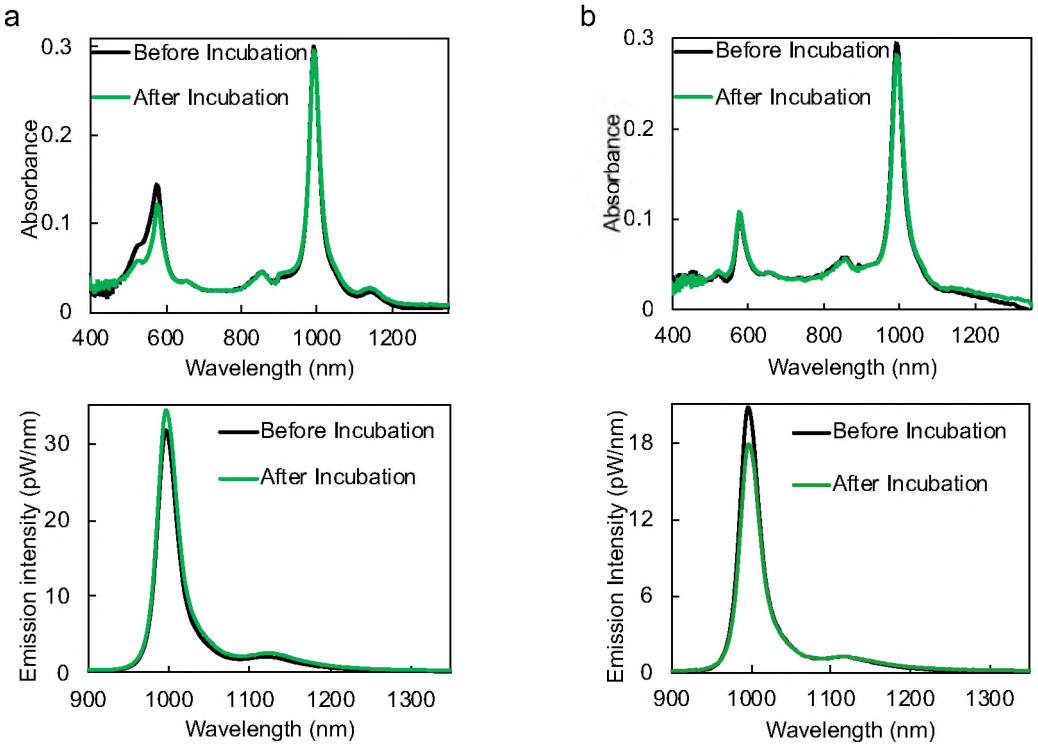

Figure 6. Absorbance and fluorescence spectra of (–) (6,5) in cell culture media with 10% FBS incubated for 8 hours at room temperature (a) and 37°C (b).

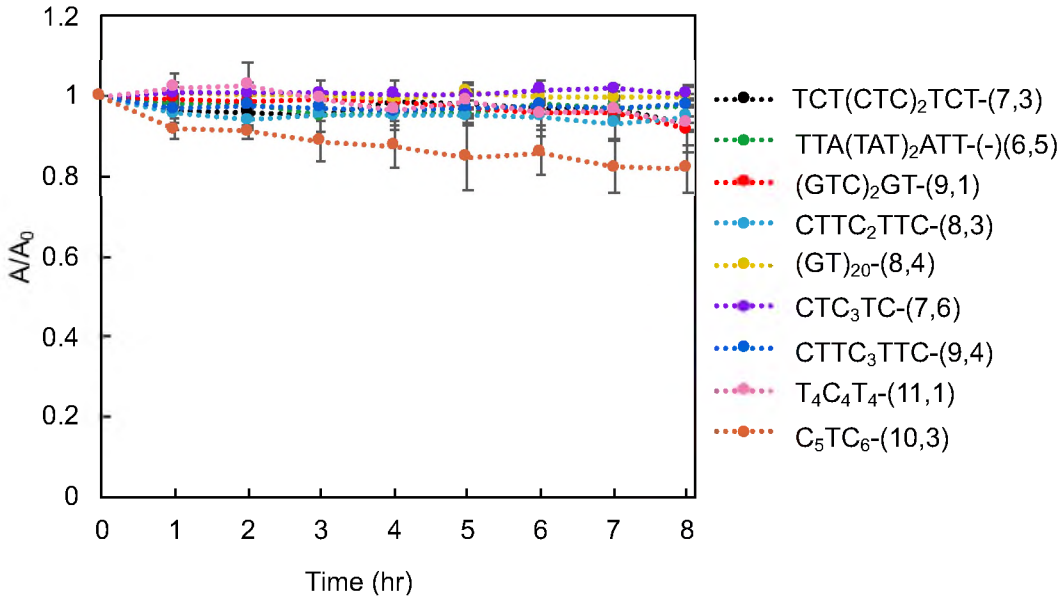

Figure 7. Absorbance ratio at E_{11} peak position of purified DNA-(*n*, *m*) SWCNT hybrids as a function of time in cell culture media with 10 % FBS at room temperature.

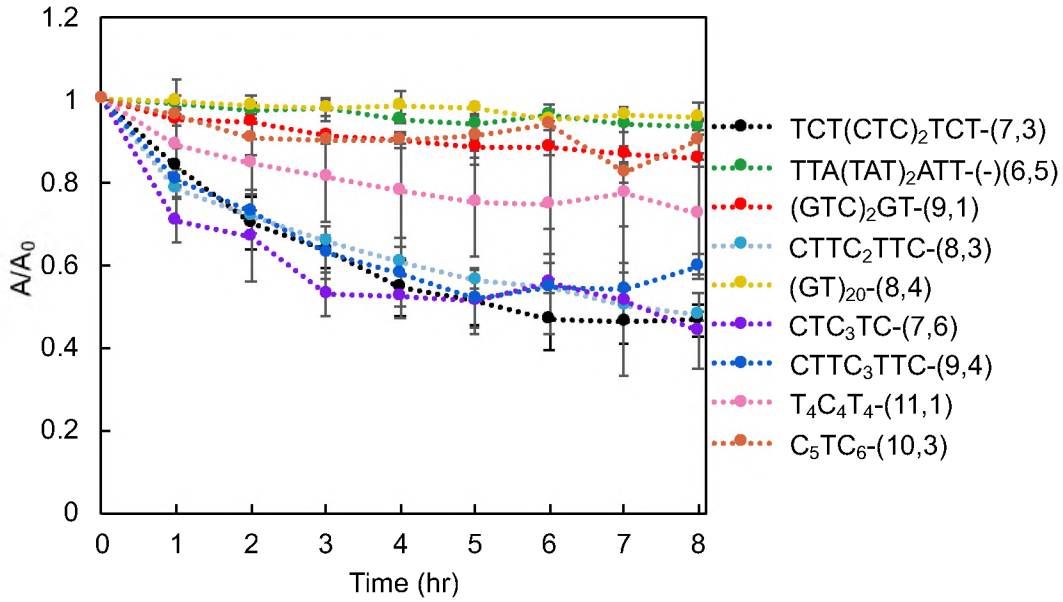

Figure 8. Absorbance ratio at E_{11} peak position of purified DNA-(*n*, *m*) SWCNT hybrids as a function of time in serum-free cell culture media at room temperature.

Appendix B

Oxygen Doping and Glycopolymer Photochemistry

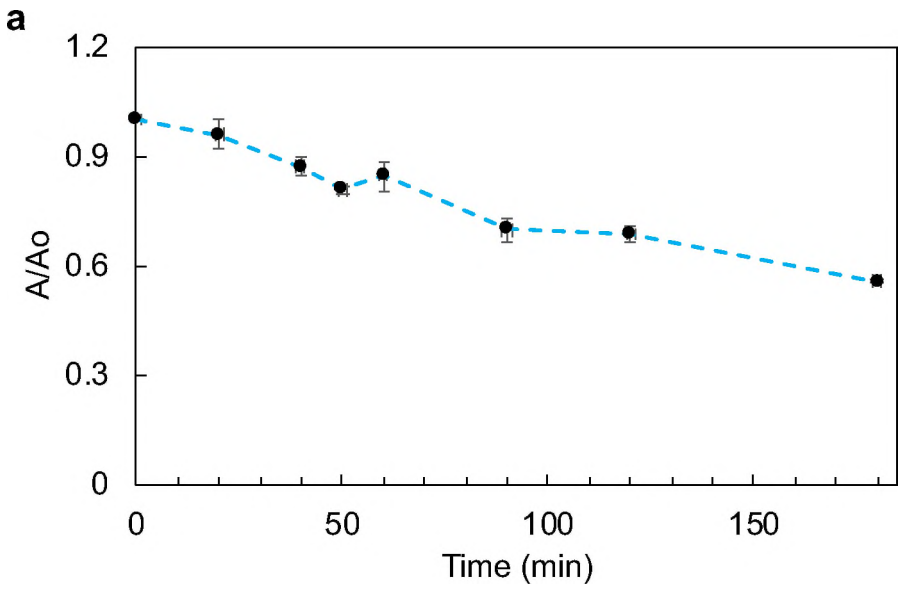

Figure 9. Dimensionless ratio for E_{11} absorbance for oxygen doped (6,5)-SDBS at different exposure times to UV 254 nm light.

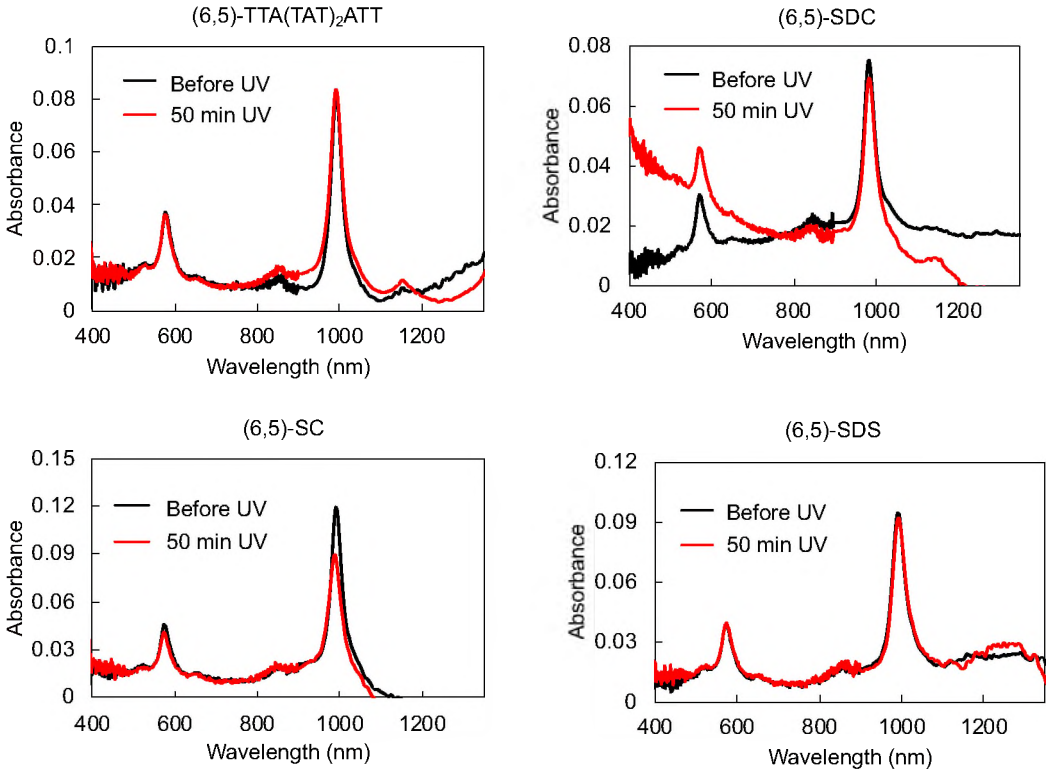

Figure 10. Absorbance spectra of (–)(6,5) SWCNT with different surface coatings, before and after exposure to UV 254 nm.

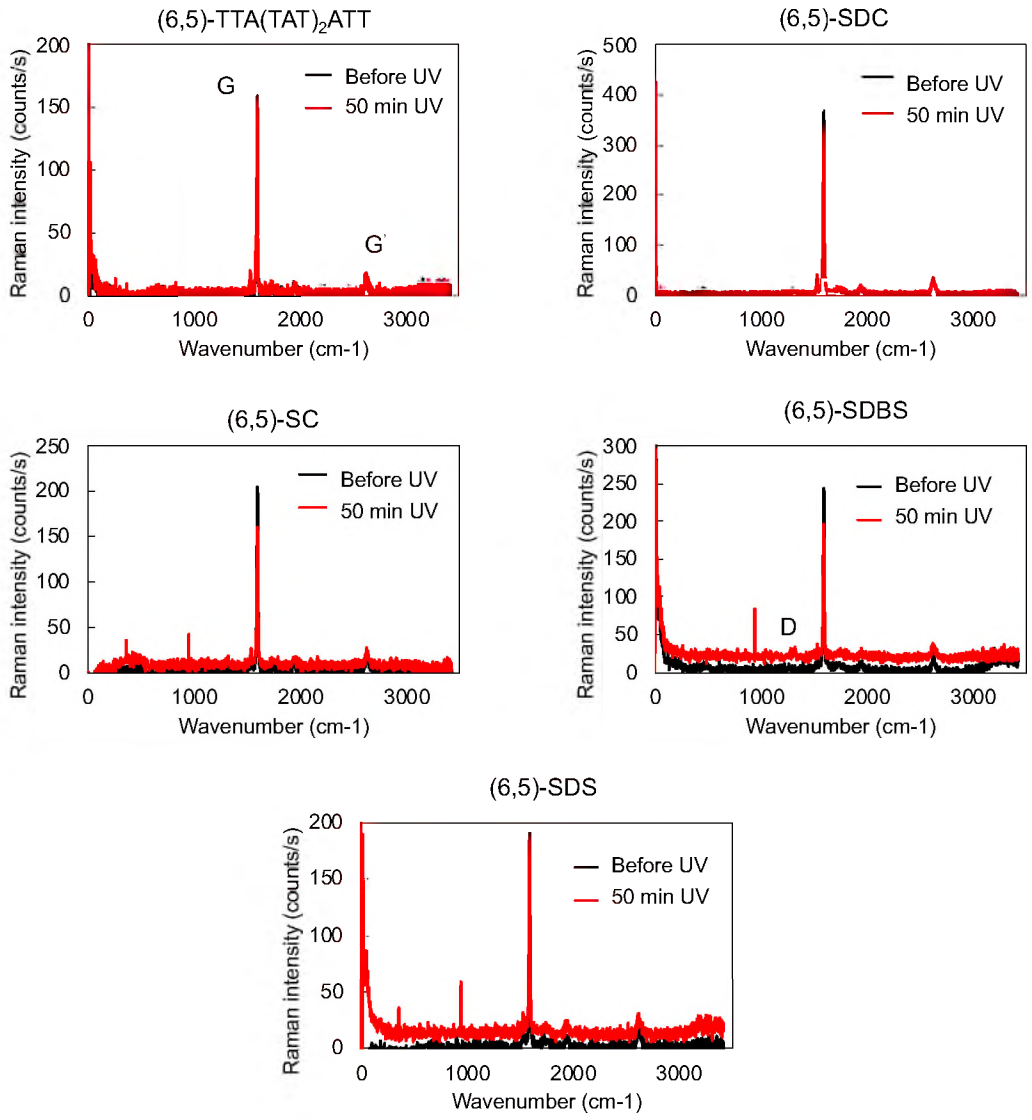

Figure 11. Raman spectra of (–)(6,5) SWCNT with different surface coatings, before and after exposure to UV 254 nm.

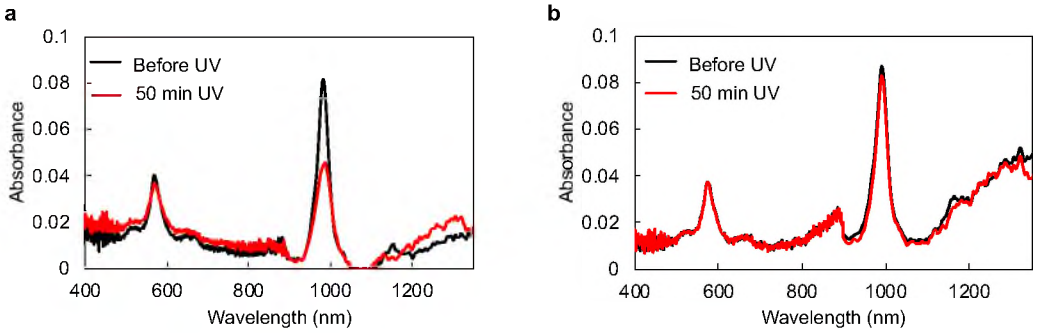

Figure 12. Absorbance spectra of (+)(6,5)-SDBS (a) and (+)(6,5)-DNA (b), before and after exposure to UV 254 nm.

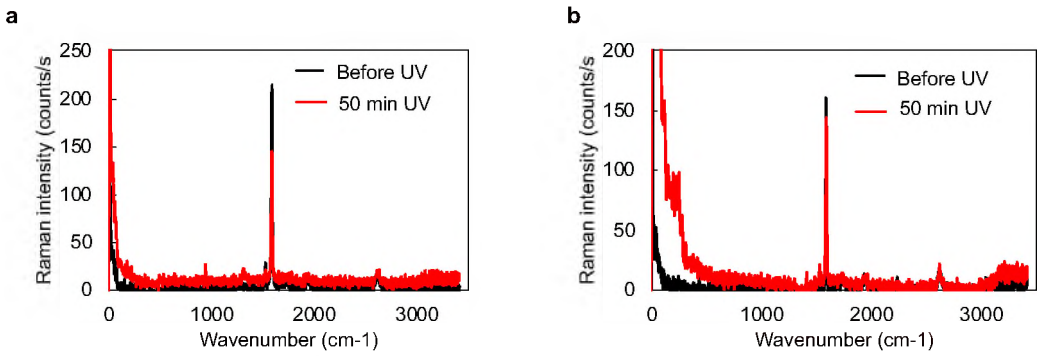

Figure 13. Raman spectra of (+)(6,5)-SDBS (a) and (+)(6,5)-DNA (b), before and after exposure to UV 254 nm.

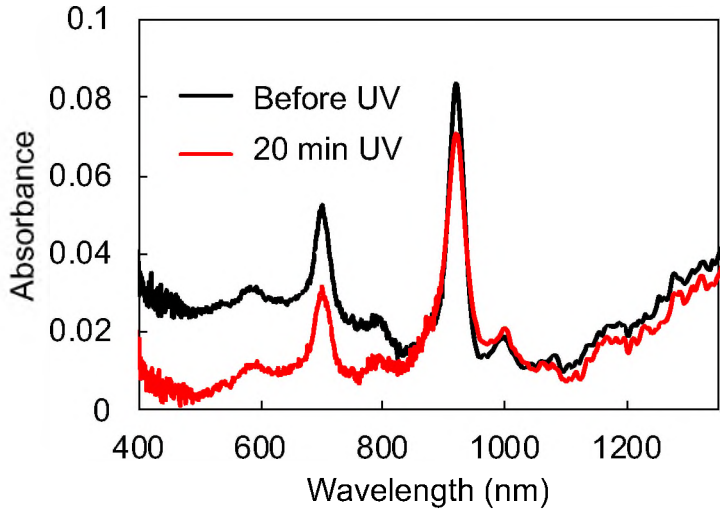

Figure 14. Absorbance spectra of (9,1)-SDBS before and after exposure to UV 254 nm.

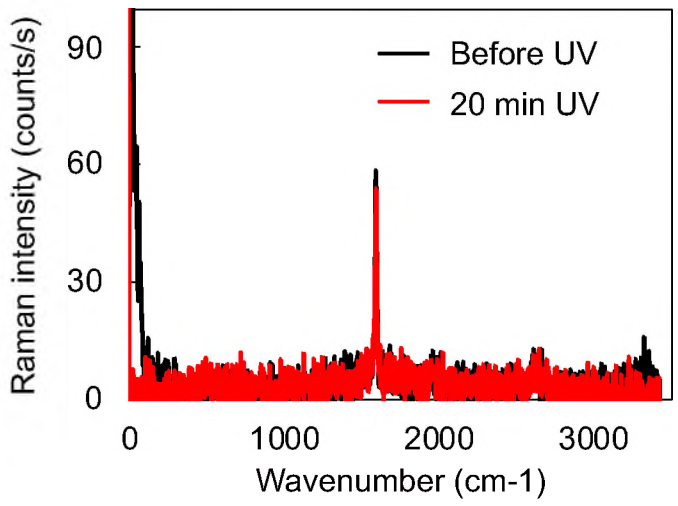

Figure 15. Raman spectra of (9,1)-SDBS before and after exposure to UV 254 nm.

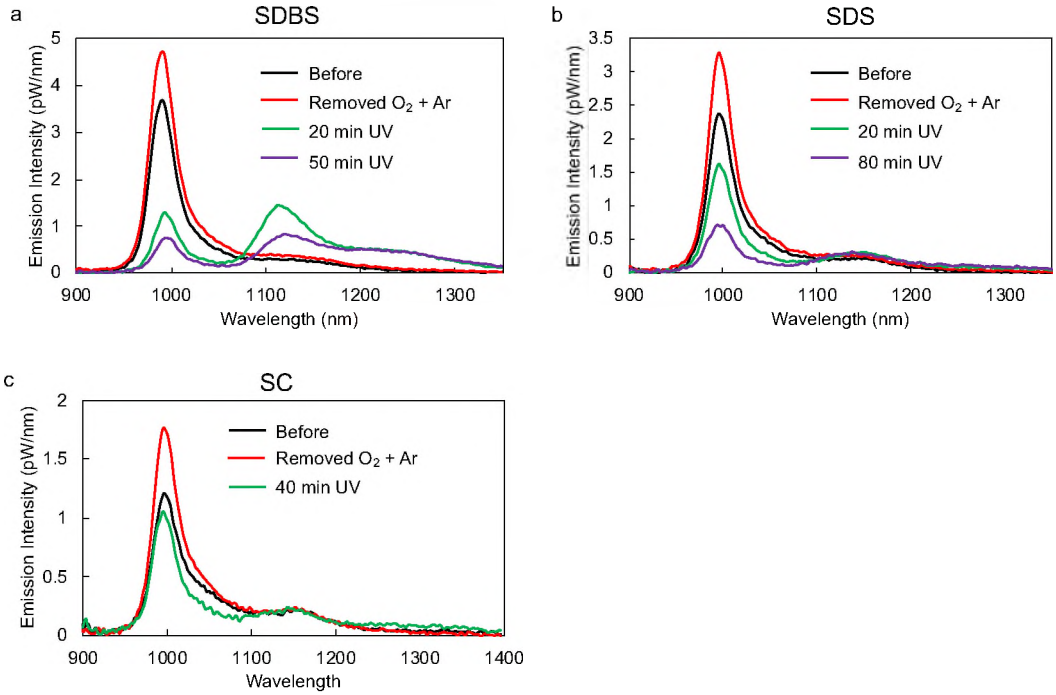

Figure 16. (–)(6,5) exposed to 254 nm UV after oxygen removal and purge with Argon gas.

Table 5. Polymer information and SWCNT:Glycopolymer mass ratios.

Glycopolymers	Polymer Characterization				SWCNT:Glyco Mass ratios
	Acrylamide *x*	Glycosylacrylamide *y*	Chain Length *n*	MW*1 (Da)	
Lact-homopolymer (0:415)	0	1	415	164.1k	1:0.3, 1:0.6
Lact-copolymer (1:1)	1	1	10	4.7k	1:0.5, 1:6
Lact-copolymer (4:1)	4	1	2	1.5k	1:0.5, 1:3, 1:6

*1. Average molecular weight determined by ^{1}H NMR spectrum of the glycopolymer

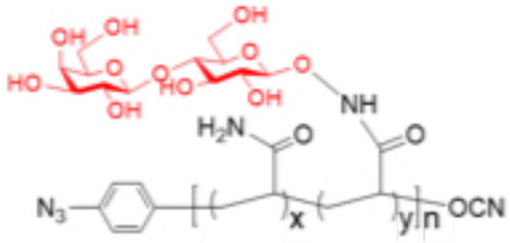

Figure 17. Glycopolymer with disaccharide lactose (Lact).

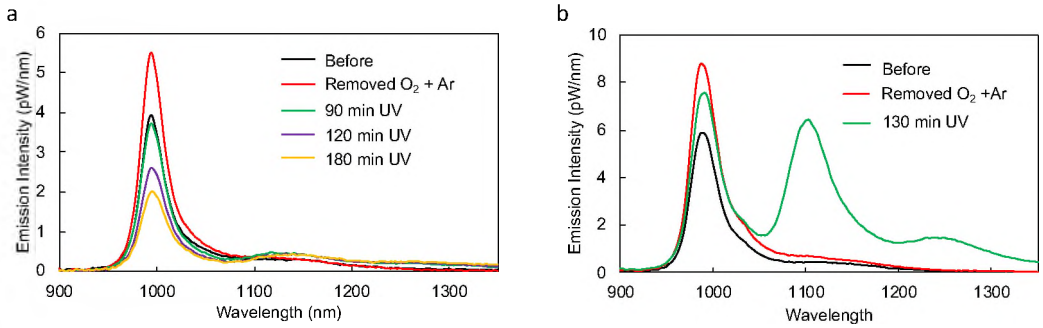

Figure 18. Blank samples of (–)(6,5)-SDS in a) D_2O and b) 1 mass % SDS-D_2O solution, for reference.